

DISSIPATION OF GROUP WAVES IN SHALLOW WATER  
FOR WAVE MODEL INPUT

A Thesis

by

DAVID ALEXANDER PAULING

Submitted to the Office of Graduate and Professional Studies of  
Texas A&M University  
in partial fulfillment of the requirements for the degree of

MASTER OF SCIENCE

Chair of Committee, James M. Kaihatu  
Committee Members, Kuang-An Chang  
Alejandro Orsi

Head of Department, Sharath Girimaji

August 2018

Major Subject: Ocean Engineering

Copyright 2018 David A. Pauling

## ABSTRACT

Surface wave data from sixteen different laboratory experiments using single and double peaked spectra was processed for wave energy spectra, shape, and dissipation parameters to describe the evolution of the double-peaked narrow-banded waves. Starting from a known model for random wave dissipation, the group waves were processed, and different regions of wave interactions were catalogued. The long wave segment of the wave groups was monitored since energy is not readily lost from long waves. The associated wave number spectra of mechanically created group waves was also determined and the corresponding wave number dependence of the spectral density compared to two theoretical values: that for the Zakharov range ( $2.5k_p \leq k \leq 1/h$ ) and for the Toba range ( $k > 1/h$ ). This comparison to these formulations for broad-banded spectra reveals whether narrow-banded wave groups can be similarly described. A time-varying dissipation mechanism was used to deduce the instantaneous energy loss from breaking; these events will also be analyzed via a probability density function and used to better model narrow-banded wave dissipation in shallow water. The trend of the most probable dissipation event was also calculated and compared to the depth. Trends of dissipation were correlated to that of the related wave energy spectra. The dependence of dissipation on higher frequencies was evaluated. The result will be useful to catalogue the dissipation of group waves.

## DEDICATION

The work here is dedicated to the Lord Jesus Christ.

## ACKNOWLEDGEMENTS

I would like to thank my committee chair, Dr. Kaihatu, for working with me the past year and half and guiding my academic career. I would also like to thank my other committee members, Dr. Kuang-An Chang and Dr. Alejandro Orsi, for being supportive during my graduate career and helping to fine tune the research conducted. I would like to thank both the ocean and civil engineering departments at Texas A&M university for being stellar in terms of nationwide standing and teaching performance throughout all my classes. Lastly I would like to thank my parents who have always encouraged and loved me throughout my life.

## CONTRIBUTORS AND FUNDING SOURCES

### **Contributors**

This work was supervised by a thesis committee consisting of Professor Kaihatu and Professor Chang of the Department of Ocean Engineering and Professor Orsi of the Department of Oceanography.

The data analyzed for Chapter 3 was provided by Dr. Ap van Dongeren, Deltares (Delft, the Netherlands) from the van Noorloos (2003) research. The code for the dispersion relation used was provided by Dr. Kaihatu of Texas A&M Civil Engineering.

All other work conducted for the thesis was completed by the student independently.

### **Funding Sources**

Graduate study was supported by the Dr. Chester P. Jelesnianski Memorial Fellowship from the Texas A&M University Department of Ocean Engineering.

## NOMENCLATURE

BC	Boundary Condition
PDF	Probability Density Function
MWL	Mean Water Level
$z$	Vertical Coordinate (negative below MWL)
$x$	Horizontal Coordinate
$t$	Time
$\omega$	Angular Wave Frequency
$T$	Wave Period
$H$	Wave Height
$\eta$	Water Elevation
$u$	Wave Velocity
$g$	Gravitational Acceleration
$k$	Wave Number
$\rho$	Water Density

## TABLE OF CONTENTS

	Page
ABSTRACT .....	ii
DEDICATION .....	iii
ACKNOWLEDGEMENTS .....	iv
CONTRIBUTORS AND FUNDING SOURCES.....	v
NOMENCLATURE.....	vi
TABLE OF CONTENTS .....	vii
LIST OF FIGURES.....	ix
LIST OF TABLES .....	xiii
CHAPTER I INTRODUCTION.....	1
1.1 Problem Statement .....	1
1.2 Boundary Value Problem .....	2
1.3 Energy .....	7
1.4 Breaking Waves .....	8
1.5 Irregular Waves .....	10
1.6 Wave Shape.....	11
1.7 Higher Order Processes .....	11
CHAPTER II DISSIPATION MODELS.....	13
2.1 Lumped Dissipation .....	13
2.2 Instantaneous Dissipation .....	14
CHAPTER III EXPERIMENT AND RESULTS.....	20
3.1 Experiment .....	20
3.2 Results .....	23
3.3 Discussion .....	37
CHAPTER IV CONCLUSION .....	42

Conclusions .....	42
REFERENCES .....	44
APPENDIX A .....	46
APPENDIX B .....	50
APPENDIX C .....	54
APPENDIX D .....	58



## LIST OF FIGURES

	Page
Figure 1: Boundary Value Problem .....	3
Figure 2: Modified Probability Density Functions Due to Wave Breaking; Reprinted from: (Thornton & Guza 1983).....	14
Figure 3: Wave Basin; Reprinted from: (van Noorloos 2003).....	21
Figure 4: Skewness and Asymmetry for A1 Group Wave.....	23
Figure 5: Skewness and Asymmetry for C1 Random Wave.....	24
Figure 6: Skewness vs $\delta$ – Group Wave Trials .....	24
Figure 7: Asymmetry vs $\delta$ – Group Wave Trials .....	25
Figure 8: Ursell # vs Skewness – Group Wave Trials .....	24
Figure 9: Ursell # vs Asymmetry – Group Wave Trials .....	25
Figure 10: Skewness vs $\delta$ – Random Wave Trials .....	25
Figure 11: Asymmetry vs $\delta$ – Random Wave Trials.....	26
Figure 12: Ursell # vs Skewness – Random Wave Trials .....	25
Figure 13: Ursell # vs Asymmetry - Random Wave Trials.....	26
Figure 14: Spectral Density for A1 Group Wave.....	27
Figure 15: Spectral Density for C1 Random Wave.....	28
Figure 16: Equilibrium Spectra for A1 Group Waves .....	29
Figure 17: Equilibrium Spectra for C1 Random Wave.....	29
Figure 18: Instantaneous Dissipation for A1 Group Wave .....	30

Figure 19: Spectral Analysis of $\epsilon$ A1 .....	31
Figure 20: PDF of $\epsilon$ Group Wave A1.....	32
Figure 21: PDF of $\epsilon$ Random Wave C1.....	32
Figure 22: Most Probable $\epsilon$ Values for Group Wave B2 .....	33
Figure 23: Probability of Most Probable $\epsilon$ for B2.....	33
Figure 24: Dissipation Rates A1 .....	34
Figure 25: Dissipation Rates C1.....	34
Figure 26: Dissipation Log Slopes A1 .....	35
Figure 27: Dissipation Log Slopes C1 .....	36
Figure 28: Averaged Log Dissipation Slopes for 9 Group Wave Trials.....	37
Figure 29: Averaged Dissipation Slopes for 6 Random Wave Trials.....	37
Figure 30: Comparison of Equation 43 to results; group wave trials.....	42
Figure 31: Comparison of Equation 43 to results; random wave trials.....	42
Figure 32: Spectral Density A1 .....	47
Figure 33: Skewness & Neg. Asymmetry A1 .....	47
Figure 34: Values of $\epsilon$ A1 .....	48
Figure 35: PDF of $\epsilon$ A1 .....	48
Figure 36: Highest Probability $\epsilon$ vs Depth A1 .....	47
Figure 37: Most Probable $\epsilon$ A1 .....	48
Figure 38: Dissipation Rate at 0.285m A1 .....	48
Figure 39: Dissipation Rate at 0.251m A1 .....	49

Figure 40: Dissipation Rate at 0.209m A1 .....	48
Figure 41: Dissipation Rate at 0.166m A1 .....	49
Figure 42: Dissipation Rate at 0.08m A1 .....	48
Figure 43: Dissipation Rates A1 .....	49
Figure 44: Log-Log Slope of Dissipation Rates A1 .....	50
Figure 45: Spectral Density B2 .....	51
Figure 46: Skewness and Asymmetry B2 .....	51
Figure 47: Values of $\epsilon$ B2.....	52
Figure 48: Probability Density Function of $\epsilon$ B2 .....	52
Figure 49: Most Probable $\epsilon$ vs Depth B2 .....	51
Figure 50: Most Probable $\epsilon$ Probability B2.....	52
Figure 51: Dissipation Rate at 0.286m B2 .....	52
Figure 52: Dissipation Rate at 0.251m B2 .....	53
Figure 53: Dissipation Rate at 0.209m B2 .....	52
Figure 54: Dissipation Rate at 0.166m B2 .....	53
Figure 55: Dissipation Rate at 0.123m B2 .....	52
Figure 56: Dissipation Rates B2.....	53
Figure 57: Log-Log Slope of Dissipation Rates B2 .....	54
Figure 58: Spectral Density C1 .....	55
Figure 59: Skewness and Asymmetry C1 .....	55
Figure 60: Values of $\epsilon$ C1.....	56
Figure 61: Probability of $\epsilon$ C1 .....	56

Figure 62: Most Probable $\epsilon$ vs Depth C1 .....	55
Figure 63: Probability of $\epsilon$ C1 .....	56
Figure 64: Dissipation Rate at 0.209m C1 .....	56
Figure 65: Dissipation Rate at 0.166m C1 .....	57
Figure 66: Dissipation Rate 0.123m C1 .....	56
Figure 67: Dissipation Rate at 0.08m C1 .....	57
Figure 68: Dissipation Rate at 0.037m C1 .....	56
Figure 69: Dissipation Rates C1.....	57
Figure 70: Log-Log Slopes of Dissipation Rate C1 .....	58
Figure 71: Spectral Density D1 .....	59
Figure 72: Skewness and Asymmetry D1 .....	59
Figure 73: Values of $\epsilon$ D1 .....	60
Figure 74: Probability Density Function of $\epsilon$ D1 .....	60
Figure 75: Most Probable $\epsilon$ vs Depth D1 .....	59
Figure 76: Probability of $\epsilon$ vs Depth D1 .....	60
Figure 77: Dissipation Rate at 0.209m D1 .....	59
Figure 78: Dissipation Rate at 0.166m D1 .....	61
Figure 79: Dissipation Rate at 0.123m D1 .....	60
Figure 80: Dissipation Rate at 0.08m D1 .....	61
Figure 81: Dissipation Rate at 0.037m D1 .....	60
Figure 82: Dissipation Rates D1 .....	61
Figure 83: Log-Log Slopes of Dissipation Rates D1 .....	62

## LIST OF TABLES

	Page
Table 1: Group Wave Parameters; Adapted from: (van Noorloos 2003).....	21
Table 2: Random Wave Parameters; Adapted from: (van Noorloos 2003) .....	21

# CHAPTER I

## INTRODUCTION

### 1.1 Problem Statement

The study of surface water wave breaking has been researched in detail concerning monochromatic and random waves, however much needs to be done connecting the two. Surface wave groups provide a middle ground with two peak frequencies, compared to fully random sea states and single frequency monochromatic wave trains. Wave groups are signals with two distinct peak frequencies both carrying a similar amount of energy. The difference in the frequency causes an envelope to form which can be used to model infra-gravity waves otherwise known as long waves.

Equation 1: Envelope Frequency

$$f_{envelope} = f_1 - f_2$$

Long waves are important in the study of coastal engineering because they drive beach morphology and the generation of sand bars. Surf beat and edge waves are formed due to the presence of higher energy long waves propagating cross shore and along shore respectively. Infra-gravity waves are generally defined as having a frequency under half the peak frequency (or a period from one to thirty minutes) and do not have a significant amount of energy until the breaking of waves occurs. There are two main interactions thought to cause this amplification of energy in long waves that is relevant to the research done in this thesis. The first is that the breaking of wave groups causes the ‘trapped’ frequency of the group envelope to become free. The second is that as the two

peak frequencies interact there is a triad interaction, or a non-linear process between three frequencies of a harmonic, that cause lower frequency waves to gain energy.

For wave groups, past research has not been done into the nature of breaking processes or dissipation of energy during breaking. Dissipation is the loss of energy during the process of breaking and will be calculated using a model based on Zelt (1991) turbulent viscosity. With the Zelt model it is possible to calculate instantaneous dissipation, denoted  $\epsilon$  in this paper, which allows the study of waves as they arrive on a case by case basis. The instantaneous dissipation gives rise to dissipation rates, denoted  $\alpha$  in this paper, which will be compared to the spectral energy plots to correlate dissipation to the spectral energy. The dissipation rates are also key to correlating earlier lumped dissipation models that focused on statistics in the wave field to the instantaneous model based on Zelt. The dissipation rates will be processed by power fitting curves, and using non-dimensional numbers used to correlate the dissipation rates to depth. The wave group dissipation analysis provides a feasible middle ground for correlating the random sea dissipation and single wave dissipation.

## **1.2 Boundary Value Problem**

To understand the dissipation of waves we must first define the basic mathematical formulations for waves, then introduce a change or loss of energy flux which will give rise to this dissipation parameter. The basic concepts found in this section will include the formulation of linear wave theory and the associated equations.

The material can be found in Dean and Dalrymple (1984) and offers a more thorough derivation.

To create the linearized equations for waves we must first define the fluid. We say that the fluid is incompressible or that density does not change a significant amount, that the fluid is Newtonian, and that the Coriolis force is neglected. We also ascribe the flow of the fluid as being irrotational. The basic boundary value problem is ordered in two dimensions such that all four sides are bounded and the inside is controlled by a governing equation. The basic terminology for these are the bottom boundary condition (BBC), Lateral boundary conditions, Dynamic free surface boundary condition (DFSBC), kinematic free surface boundary condition (KFSBC), and the Laplace equation described after the figure as the governing equation.

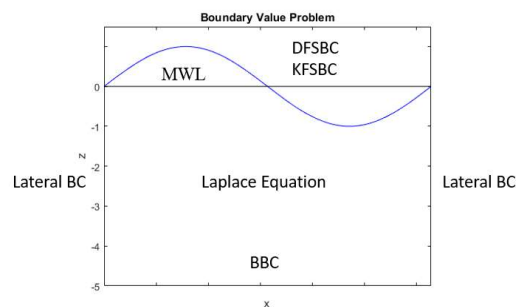


Figure 1: Boundary Value Problem

where MWL is the mean water level and is on  $z$  equal zero. In the study of wave mechanics an important concept is needed to reduce the number of variables present in a problem and adequately describe the motions of the fluid. This concept is called the velocity potential and takes the directionality out of the velocity components by



integrating each direction and combining them as a coordinate vector. The velocity potential has been shown in numerous studies to adequately model physical wave phenomenon. The basic definition of the velocity potential is shown below.

Equation 2: Velocity Potential

$$\nabla\phi = u$$

To determine the value for the velocity potential as it pertains to waves we must define the boundaries of the fluid and the processes that govern the fluid inside the boundaries. For inside the boundaries we use a conservation of mass equation, from classical physics, and then due to the unchanging density of the fluid the subsequent result is the Laplace Equation shown as equation 3.

Equation 3: Laplace Equation

$$\nabla^2\phi = 0$$

where  $\nabla$  denotes a gradient derivative. Now we need to define the boundaries of the problem. The side boundary conditions or lateral boundaries need to have the wave repeat in time and space so that there is a propagation of the wave as the physical phenomenon occurs. This condition will be satisfied using trigonometric functions. The bottom boundary for linear waves simply states that the fluid does not pass through the floor, so we assume that there is no permeability and that the vertical velocity at the floor is zero. Mathematically it is shown below as equation 4.

Equation 4: Bottom Boundary Condition

$$\frac{\partial\phi}{\partial z} = 0$$

where  $z$  is a vertical direction described by figure 1. The kinematic free surface boundary condition arises from the motion of the fluid at the interface between the air and water. Since the density of air is much smaller than that of water we neglect its importance for linear waves. The KFSBC also assumes that the water at the surface will stay there and not be displaced into the water column. The dynamic free surface condition is satisfied by a constant free surface pressure that is present due to gravity. For linear theory these boundary conditions reduce to equations 5 and 6.

Equation 5: Kinematic Free Surface Boundary Condition

$$\frac{\partial \eta}{\partial t} = \frac{\partial \phi}{\partial z}$$

Equation 6: Dynamic Free Surface Boundary Condition

$$g\eta = \frac{\partial \phi}{\partial t}$$

where  $\eta$  is the wave elevation,  $t$  is time,  $\phi$  is the velocity potential,  $g$  is gravity, and  $\delta$  denotes a partial derivative. With the full problem laid out we can solve for the free surface elevation and velocity potential. The method of separation of variables is used to set up two linear differential equations, one for the  $x$  direction and one for the  $z$  direction. Resolving these gives us the velocity potential for linear waves shown below.

Equation 7: Linear Velocity Potential

$$\phi = -\frac{iga}{2\omega} * \frac{\cosh(k(h+z))}{\cosh(kh)} * e^{i\theta}$$

Equation 8: Linear Free Surface Elevation

$$\eta = a * e^{i\theta}$$

where  $i$  is an imaginary number,  $g$  is the gravitational constant,  $a$  is the amplitude of the wave, and  $\theta$  is the wave phase. The wave phase can also be described as a function of the wave number and the wave frequency as shown in the equation below.

Equation 9: Wave Phase

$$\theta = kx + \omega t$$

From the resolution of the velocity potential, there needs to be a solvability condition, which can take three forms. One is a trivial solution where there is no motion, one has negative solutions for the wave number, which make the solution imaginary and the third is the only one that makes sense in the physical world and we call it the dispersion relation, which relates the wave number to the wave frequency and water depth. With this condition having any of the two of those lets us solve for the third.

Equation 10: Dispersion Relation

$$\omega^2 = gk * \tanh(kh)$$

where  $\omega$  is the angular wave frequency,  $k$  is the wave number, and  $h$  is the depth. The wave celerity,  $C$ , is defined as the speed at which the wave progresses and is simply defined as follows.

Equation 11: Wave Celerity

$$C = \frac{\omega}{k}$$

### 1.3 Energy

The energy of an approaching wave can be split into two main mechanical parts, potential and kinetic energy. Each of these has an equal contribution in linear wave theory. The potential energy is derived from the difference from the still water level to the height of the wave whereas the kinetic energy is found based on the particle velocities of the wave.

Equation 12: Kinetic and Potential Energy

$$KE = PE = \frac{1}{16} * \rho g H^2$$

where  $KE$  is the kinetic energy,  $PE$  is the potential energy, and  $H$  is the wave height. Energy flux (as it applies to waves) is defined as the amount of energy moving through an area per unit time. For linear wave theory it is derived from the dynamic pressure difference times the velocity, averaged by space and time. The resulting equation becomes the group velocity multiplied by the total energy. The group velocity is a measure of how fast energy is carried in a wave.

Equation 13: Wave group velocity

$$C_g = n * C$$
$$n = \frac{1}{2} * \left( 1 + \frac{2kh}{\sinh(2kh)} \right)$$

Thus, the average energy flux can be derived by averaging in time and space and is shown below.

Equation 14: Averaged Energy Flux

$$\mathcal{F} = E * C_g$$

Unless there is a process added into the system the change in energy flux for waves is always zero. The process of shoaling for surface waves involves the increase in wave height as a response to the decrease in water depth, due to the conservation of energy flux before the waves break. Since the water does not change density and the depth is decreasing as the wave approaches shore, the wave height must increase to balance the energy flux, which leads to the relation.

Equation 15: Pure Shoaling

$$H_2 = H_1 * \sqrt{\frac{C_{g1}}{C_{g2}}}$$

#### **1.4 Breaking Waves**

It is important to note that so far the conditions and equations do not account for breaking of waves. The velocity potential that describes waves in linear wave theory does not account for wave breaking. Physically waves seem to ‘topple over’ and form turbulent eddies once a certain unstable wave height is reached. From observations in the physical world it appears that waves reach this height, which we call the breaking wave height, and then break and experience a loss of energy due to the turbulent processes present. The loss of energy can be characterized as a dissipation parameter that will be described by models detailed in chapter 2. Wave breaking is important to coastal sediment processes due to the energy being lost being ‘injected’ into the bed. Formulations have been done in the past to characterize the breaking process.

McCowan (1894) used solitary wave theory analysis to show that wave heights have an upper bound that is a constant ratio to the water depth as shown below.

Equation 16: McCowan Wave Breaking

$$\frac{H_b}{h_b} = 0.78 = \kappa$$

where  $\kappa$  is a non-dimensional breaking parameter and the subscript  $b$  denotes the breaking value. Weggel (1972) derived a dependency on the water depth and beach slope where his results are,

Equation 17: Weggel Wave Breaking

$$\kappa = b(m) - a(m) * \frac{H_b}{gT^2}$$

$$a(m) = 43.8(1 - e^{-19m}) \quad ; \quad b(m) = 1.56(1 + e^{-1.5m})^{-1}$$

where  $m$  is the slope of the beach. Interestingly the function proposed by Weggel asymptotically approaches a  $\kappa$  value of 0.78 which matches the study done by McCowan almost a century prior.

In this research the energy flux balance is taken to be equal to a dissipation parameter which will govern the energy lost during wave breaking. Wave breaking has important concepts in coastal engineering one of these being the movement of energy from the waves into the bed causing sediment transfer. The breaking process also incurs a mean sea level increase in the breaker and swash zones. To adequately describe the breaking process as instantaneous dissipation function, a model will be used and its mathematical form is described in the next chapter.

## 1.5 Irregular Waves

Typical waves observed in nature do not have a single wave height or period. Research by Longuet-Higgins (1952) showed that irregular sea states could be described by statistical analysis, specifically with a Rayleigh distribution. The Rayleigh distribution is a statistical distribution of positive numbers that crosses the origin and has a single peak. A Rayleigh distribution was used for the probability of wave heights occurring. Since wave height cannot be a negative value and previous research concluded that waves are single-peaked in nature this is one valid wave model.

More recent research has incorporated Fourier transforms to describe how each frequency carries a different amount of energy (or each has a different wave height). This analysis can be compared to the statistics of the Rayleigh distribution of wave heights by using the area under the spectrum to be equal to a zeroth moment then using known relations between this and other statistics such as root mean square wave height and significant wave height (average of the top third of waves). The process can also be reversed in which multiple frequencies of waves are superimposed to simulate the random waves observed.

Smith and Vincent (2003) developed an expression to describe the equilibrium conditions of waves nearshore. To describe the power law of the spectra, a transformation was used to calculate an Equilibrium spectrum, which correlates wave number,  $k$ , to energy instead of frequency to energy. Then based on the work by Zakharov (1999) and Toba (1973) different wave number ranges were developed based around the peak wave number,  $k_p$ . Toba indicated that high wave number components

could be fit by a  $-5/2$  power law, which is now called the Toba range. Zakharov proposed a  $-4/3$  power law in areas of small relative water depth,  $kh$ , now called the Zakharov range. From experiment it seems that  $k$  values ranging from  $2.5k_p$  to  $k = 1/h$  fit the Zakharov range and values of  $k > 1/h$  fit the Toba range. These power laws and ranges thereof can be used to predict equilibrium spectral shapes.

## 1.6 Wave Shape

Waves governed by linear theory form perfect sinusoidal shapes from deep to shallow water, which is not expressed in the physical phenomena. To describe the changing shape of the waves we implore statistical quantities such as skewness which measures the difference from the front and back of a crest and asymmetry which measures the difference in the wave above and below the mean water level. These differences in the characteristic shape of waves govern a mean water and sediment transport. Waves in shallow water have more of a saw tooth pattern than an actual sinusoid which causes linear theory to be inadequate to describe the processes involved. This steep edge on the front face of a wave can lead to increased impact forces with a structure. Bailard (1981) showed that this saw-tooth pattern led to the generation of sand bars due to the cross-shore sediment transport created. Mathematical formulations to describe the shape of waves will be discussed in chapter 3.

## 1.7 Higher Order Processes

The introduction of higher order processes account for multiple new quantities that are observed in the wave field. Higher order processes are called such due to the



boundary conditions keeping terms that are multiplied by each other. The existence of set up and set down, a change in the MWL, can be calculated using a higher order theory. Shallow water waves need higher order processes to adequately describe their shape and harmonic triad interactions. Harmonic triads occur when two different frequencies interact to generate a third frequency. The change in wave shape due to shoaling and varying bathymetry can also be accounted for using a higher order theory. This change can be calculated using the skewness and asymmetry of the waves, which are both equal to zero for the case of linear waves. Particle velocities of linear waves form closed circuits which in turn leads to a net mass transport of zero. Using a second or higher order theory the particles have a slow drift towards shore which can account for accumulation of sediment and set-up of the mean water level. Wave breaking still cannot be described by using a higher order theory, rather a model for dissipation of energy is needed.

## CHAPTER II

### DISSIPATION MODELS

#### 2.1 Lumped Dissipation

Breaking is easily observable in nature but hard to quantify theoretically. In physical scenarios the waves can be seen “toppling over” or “plunging” into the ocean which leads to smaller amplitude waves. Breaking is usually modeled as occurring after a certain wave height is exceeded, called the breaking wave height. The breaking process causes energy loss, which is called dissipation. Early work into the dissipation of waves used a lumped dissipation parameter and would cut off waves after they exceeded the breaking height or shortly after exceedance. Breaking involves the turbulent processes under which a wave loses energy and subsequently loses wave height. Early study used the example of a turbulent bore to model the processes involved during breaking. All methods to quantify the lumped breaking process are from empirical formulations and assume a probabilistic nature. The lumped parameter methods assume a Rayleigh distribution in the probability of wave heights occurring and are trying to best fit curves to the data available at the time. Lumped dissipation mathematically can be shown as the total change in energy flux over the breaking zone is equal to a constant, shown below.

Equation 18: Lumped Dissipation

$$\frac{\partial \mathcal{F}}{\partial x} = -\epsilon$$

where  $\mathcal{F}$  is the averaged energy flux of the wave and  $\epsilon$  is the lumped dissipation or total energy loss due to breaking. The figure below from Thornton and Guza (1983)

shows the general idea behind each traditional method of cataloguing dissipation by various authors.

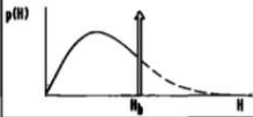
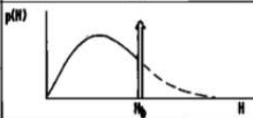
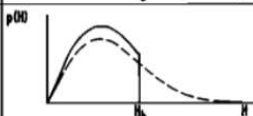
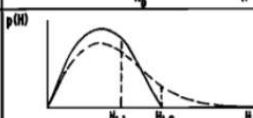
AUTHOR	DISTRIBUTION	SHOALING	BREAKER CRITERIA
COLLINS (1970)		LINEAR	$\frac{H_b}{H_d} = 0.76\beta^{1/7} (H_d/L_d)^{-1/4}$ (AFTER LAHAYE AND NGH, 1967)
BATTJES (1972)		LINEAR	$H_b = \frac{0.68}{k} \tanh\left(\frac{\gamma}{0.68} kh\right)$
KUO and KUO (1974)		LINEAR	$H_b = 0.63h$
GODA (1975)		NONLINEAR (SHUTO, 1974)	$\frac{H_b}{H_d} = \frac{L_d}{h} \left[ 1 - \exp\left\{-1.5 \frac{h}{L_d} (1 + 4 \tan^2 \beta)\right\}\right]$ (AFTER GODA, 1975)

Figure 2: Modified Probability Density Functions Due to Wave Breaking; Reprinted from: (Thornton & Guza 1983)

Lumped dissipation does accurately show the mean effects of wave breaking in the coastal zone but does not account for a wave-by-wave basis. Individual waves will need a different formulation to describe the dissipation processes involved.

## 2.2 Instantaneous Dissipation

Kaihatu et al. (2007) proposed a different model for wave dissipation. They proposed that the shape and energy content in ocean surface waves in the surf zone impose a framework for dissipation in the surf zone. Surf zone waves are normally characterized by large negative values for asymmetry and large positive values for skewness during breaking which leads to a saw tooth wave shape. Processes such as

shoaling, breaking, and nonlinear interactions between triads of waves tend to shape the wave characteristics as the waves approach shore. Unlike previous work (Collins (1970), Battjes (1972), Kuo and Kuo (1974), Goda (1975), and Thornton & Guza (1983)) which use the lumped dissipation method by calculating average dissipation characteristics, the method described by Kaihatu et al. (2007) features statistical quantities such as skewness and asymmetry and has a time or frequency dependence. Due to dissipation being based on shoaling and wave triad interactions as well as breaking, the waves inject dissipation of energy slowly into the system as opposed to only at breaking. The reason behind this is that triad interactions in waves create a more peaked energy spectrum in the second harmonic which results in a non-narrow or wide banded spectrum. This also has the effect that waves will not break at one depth but over a range of depths, due to possible significant energy in multiple frequencies. The complex wave amplitude can be used as a representation of dissipation wave transformation model as shown below.

Equation 19

$$\frac{\partial A_n}{\partial x} = -\alpha_n A_n$$

where  $A_n$  is the complex amplitude and  $\alpha_n$  is an assumed dissipation rate parameter that is dependent on the frequency relative to its energy spectrum counterpart. Chen et al (1997) described an asymptotic behavior of the dissipation parameter  $\alpha_n$  dependence on frequency squared. This results in good approximate wave shape calculated by the related skewness and asymmetry. With this relation of complex amplitude to dissipation we can now describe an energy flux balance as,

Equation 20: Evolution Equation

$$A_n + \frac{1}{2C_{gn}} * \frac{\partial C_{gn}}{\partial x} A_n = \alpha_n A_n$$

Which includes now the group velocity of the wave  $C_{gn}$ . This equation is also sometimes referred to as an evolution equation because it describes the evolution of wave shape and amplitude from deep to shallow water. To quantify the dissipation rate, it is necessary to adopt a dissipation model for wave breaking conditions. Zelt (1991) proposed a model based on the combined free surface boundary condition including eddy viscosity as,

Equation 21: Combined Free Surface Boundary Condition

$$\frac{\partial u}{\partial t} + u \frac{\partial u}{\partial x} + g \frac{\partial \eta}{\partial x} + R - \frac{\partial \left( v_b \frac{\partial u}{\partial x} \right)}{\partial x} = 0$$

where  $v_b$  is the eddy viscosity and  $\delta$  denotes derivatives with the respective direction,  $x$ , or time,  $t$ . A closure model for the eddy viscosity is needed and Zelt (1991) also developed the expressions,

Equation 22: Zelt Eddy Viscosity

$$v_b = -Bl^2 \frac{\partial u}{\partial x}$$

Equation 23: Zelt Mixing Length

$$l = \gamma(h + \eta)$$

Which allows the breaking type to be based on the  $B$  value. The mixing length parameter,  $\gamma$  was found to be equal to two from experimental data. The Zelt model uses the same McCowan (1894) relation of a constant ratio between wave height and water

depth. Since  $B$  values are based on the breaking type, a breaking model is assumed to be dependent on the velocity of the crest compared to a critical velocity of breaking as,

Equation 24: Critical Breaking Velocity

$$u_x^* = -0.3\sqrt{g/h}$$

Equation 25: Breaking Conditions

$$B = 1; u_x \leq 2u_x^*$$

$$B = \frac{u_x}{u_x^*}; 2u_x^* < u_x \leq u_x^*$$

$$B = 0; u_x > u_x^*$$

where for convenience the subscripts  $x$  and  $t$  are partial derivatives for the  $x$  direction and time respectively. These equations use the steepness of the front face of the waves to determine the eddy viscosity. These parameters are not easily calculated from gauge data since usually the gauges have a sampling rate and vary with time while being in a fixed space. This means that spatial derivatives are not optimal for real world data processing applications. Instead a first order approximation developed by Kennedy et al (2000) is used to transform  $B$  into,

Equation 26: Linear Relation

$$u_x = \frac{\eta_t}{h}$$

Equation 27: Eddy Viscosity

$$v_b \approx B\gamma^2 h \eta_t$$

Equation 28: Critical Breaking Elevation

$$\eta_t^* = 0.3\sqrt{gh}$$

Equation 29: Breaking Conditions

$$B = 1; \eta_t \leq 2\eta_t^*$$

$$B = \frac{\eta_t}{\eta_t^*} - 1; 2\eta_t^* < \eta_t \leq \eta_t^*$$

$$B = 0; \eta_t > \eta_t^*$$

This allows the instantaneous energy dissipation,  $\epsilon_b$  expressed by Kaihatu et al. (2007) to be rewritten as,

Equation 30: Instantaneous Energy Dissipation

$$\epsilon_b = -\rho hu(v_b u_x)_x \approx -\rho \left(\frac{\eta}{h}\right) (v_b \eta_t)_t$$

Inference of the instantaneous energy dissipation from field measurements is now simple to calculate at each sensor. A relationship between the statistics of this parameter with the Rayleigh lumped dissipation parameter methods could also be done to validate the instantaneous method. More work is needed to know the dependence of energy dissipation on frequency, or in other words to calculate  $\alpha_n$ . Using the energy flux balance from above and the spectral densities of the wave heights and instantaneous energy dissipation rate,  $\alpha_n$  is shown to be,

Equation 31: Energy Dissipation Rate

$$\alpha_n = \frac{1}{\rho g \sqrt{gh}} * \frac{1}{\sqrt{2\Delta f}} * \frac{\sqrt{S_{\epsilon_b}(n)}}{S_\eta(n)}$$

where  $\Delta f$  is the sampling rate and  $S_\eta(n)$  and  $S_{\epsilon_b}(n)$  are as follows,

Equation 32: Wave Energy Spectra

$$S_\eta(n) = \frac{\langle |A_n|^2 \rangle}{2\Delta f}$$

Equation 33: Dissipation Spectra

$$S_{\epsilon_b}(n) = \frac{\langle |\epsilon_{bn}| \rangle^2}{2\Delta f}$$

Thus from any wave signal it is possible to calculate instantaneous energy dissipation as a result of the change in wave elevations and also the dependency of the frequency on dissipation. Since the  $S_{\epsilon_b}$  has little to no dependence on frequency we can conclude that  $\alpha_n \propto S_\eta(n)^{-1}$  or  $\alpha_n \propto f^2$  asymptotically as discovered in earlier studies. This model for dissipation is assuming significant asymmetry and no skewness, whereas in actuality both skewness and asymmetry will be present in a shallow water wave field in the surf zone. Slopes of  $\alpha$  and the wave energy spectra can be calculated and compared using the above techniques.

The comparison to earlier work will be done using a histogram function in Matlab and setting the bin size to one integer value of  $\epsilon$ , the instantaneous energy dissipation. This will create a probability density function of the instantaneous dissipation and since the range of  $\epsilon$  is in the order of thousands then an integer value for bins should be adequate in resolution. This should be a viable method of tying together and comparing the lumped dissipation methods with the instantaneous method.



CHAPTER III  
EXPERIMENT AND RESULTS

**3.1 Experiment**

The data used in this research was collected in the wave flume at the Fluid Mechanics Laboratory at the Technical University of Delft (van Noorloos 2003). The wave basin used for this experiment has a fixed sloping bottom at a 1/35 incline and the length is 33 meters. A hydraulically driven piston type wave maker was used to generate the wave groups and random waves. Multiple gauges were setup throughout the wave flume to capture the time series data at fixed locations with a sampling rate of 25 Hz. A total of fifteen trials will be used in this paper, six for random waves and nine for group waves. The random waves were generated using random realizations of a JONSWAP spectrum with the peak frequency and associated wave height properties shown in table 2. below is a graph of the experiment (with all values in meters) and two tables of the wave heights and frequencies associated with each trial from van Noorloos (2003).

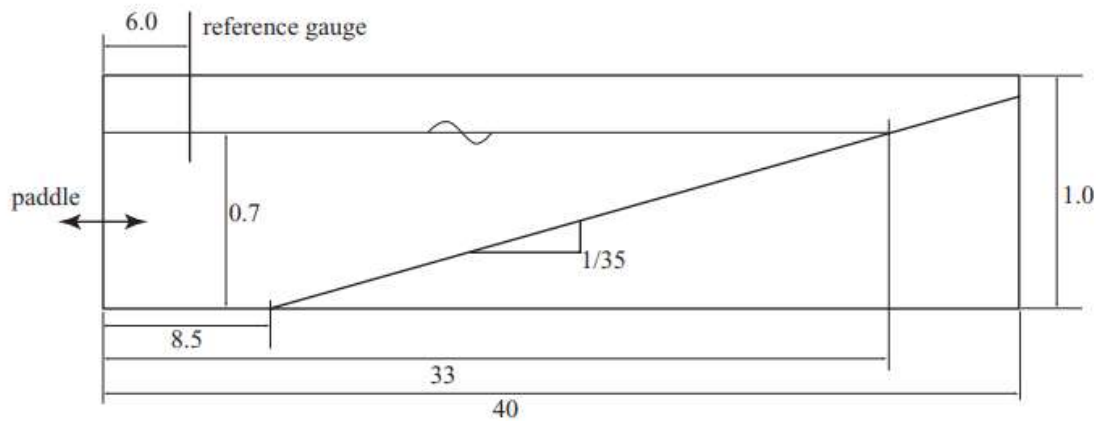


Figure 3: Wave Basin; Reprinted from: (van Noorloos 2003)

Experiment	A1 (m)	A2 (m)	Freq1 (Hz)	Freq2 (Hz)
A1	0.06	0.012	0.6714	0.4761
A2	0.06	0.012	0.647	0.5005
A3	0.06	0.012	0.6348	0.5127
A4	0.06	0.012	0.6226	0.5249
A5	0.06	0.012	0.5859	0.5615
B1	0.06	0.012	0.647	0.5
B2	0.06	0.018	0.647	0.5
B3	0.06	0.024	0.647	0.5
B4	0.06	0.03	0.647	0.5
B5	0.06	0.036	0.647	0.5

Table 1: Group Wave Parameters; Adapted from: (van Noorloos 2003)

Experiment	$H_{mo}$ (m)	Freq (Hz)	Duration (min)
C1	0.05	0.5	40
C2	0.075	0.5	40
C3	0.1	0.5	40
D1	0.05	0.65	31
D2	0.075	0.65	31
D3	0.1	0.65	31

Table 2: Random Wave Parameters; Adapted from: (van Noorloos 2003)

Statistical quantities such as skewness and asymmetry are useful for explaining the changing shape of waves and are defined mathematically as follows. Positive skewness is interpreted as the wave crest leaning forward causing a steeper front face and positive asymmetry is physically the wave carries more water above the MWL.

Equation 34: Skewness

$$Skewness = \frac{\langle \eta^3 \rangle}{\langle \eta^2 \rangle^{\frac{3}{2}}}$$

Equation 35: Asymmetry

$$Asymmetry = \frac{\langle \mathcal{H}(\eta)^3 \rangle}{\langle \eta^2 \rangle^{3/2}}$$

where  $\eta$  is the wave elevation and  $\mathcal{H}$  denotes the Hilbert transform. Some other useful statistical quantities to further quantify the differences between random and group waves are the root mean square wave height, the relative wave height, the relative water depth, and the Ursell number all defined below.

Equation 36: Root Mean Square Wave Height

$$H_{rms} = \sqrt{\langle \eta^2 \rangle}$$

Equation 37: Relative Wave Height

$$\delta = \frac{H_{rms}}{h}$$

Equation 38: Relative Water Depth

$$rel. \text{ water depth} = kh$$

Equation 39: Ursell Number

$$ursell \# = \frac{\delta}{(kh)^2}$$

These are useful in categorizing the different stages a wave has as it approaches the shore. The waves exhibit behaviors that are unique to the processes before, during and after breaking.

### 3.2 Results

Statistical quantities describing the dissipation and various terms associated were found. First the skewness and asymmetry for the random and group waves was calculated and compared to each other. The graphs show to the range of depths at which the waves break.

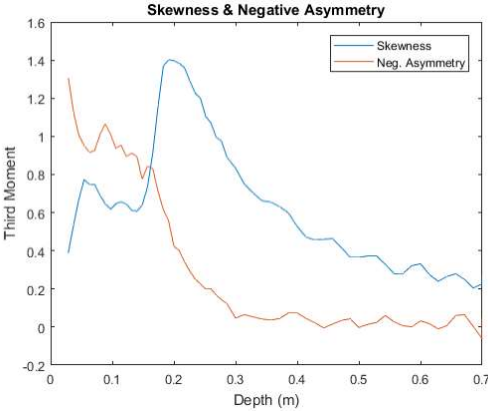


Figure 4: Skewness and Asymmetry for A1 Group Wave

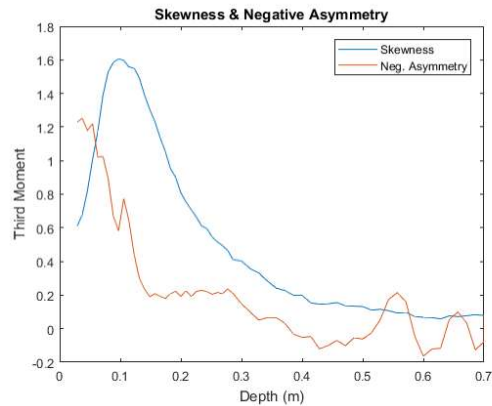


Figure 5: Skewness and Asymmetry for C1 Random Wave

The results show that for random waves the maximum skewness and asymmetry happen at much shallower water with only one peak. For group waves the graph is different; the waves first break further offshore and then stabilizes before breaking again in very shallow waters. The skewness and asymmetry were then compared to other dimensionless parameters such as root mean square wave height, relative wave height, relative wave steepness, and Ursell number. These were compared to the skewness and asymmetry to further map the processes of dissipation and the resultant effect on these statistics. These are graphed versus the skewness and asymmetry shown below and showcase the three modes before, during, and after breaking.

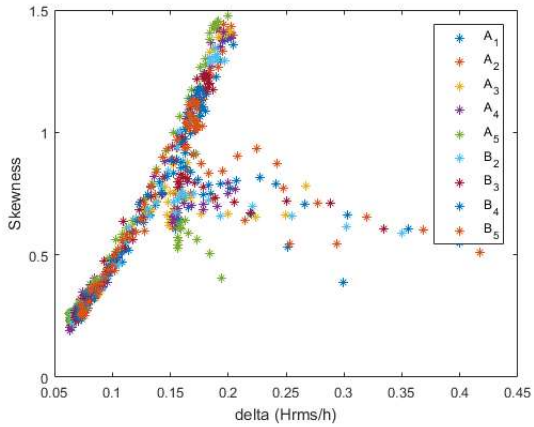


Figure 6: Skewness vs  $\delta$  – Group Wave Trials

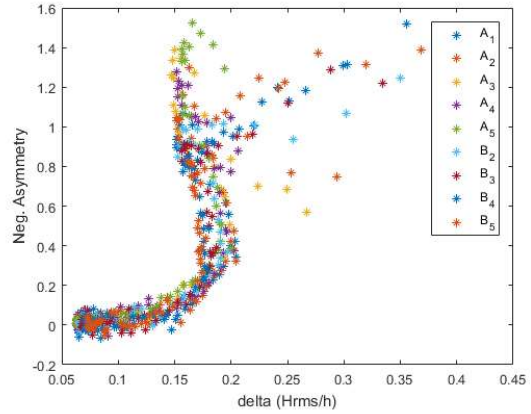


Figure 7: Asymmetry vs  $\delta$  – Group Wave Trials

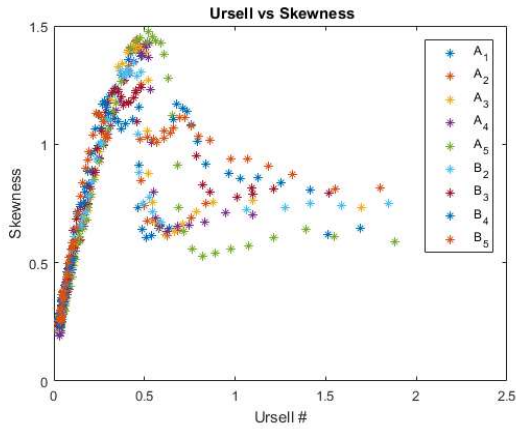


Figure 8: Ursell # vs Skewness – Group Wave Trials

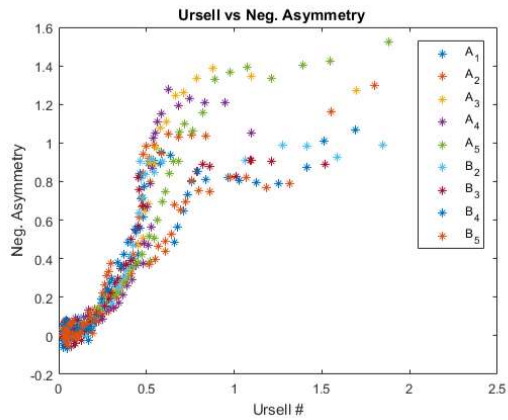


Figure 9: Ursell # vs Asymmetry – Group Wave Trials

For the wave groups in figure 6 and 8,  $\delta$  and Ursell number are compared to skewness and there is an increase in the skewness of the wave as it approaches shallower water, then after breaking the skewness appears to decrease rapidly and then stabilize at a less steep front face of the wave. In figures 7 and 9,  $\delta$  and Ursell number are compared to the asymmetry which tends to always become more negative as depth decreases.

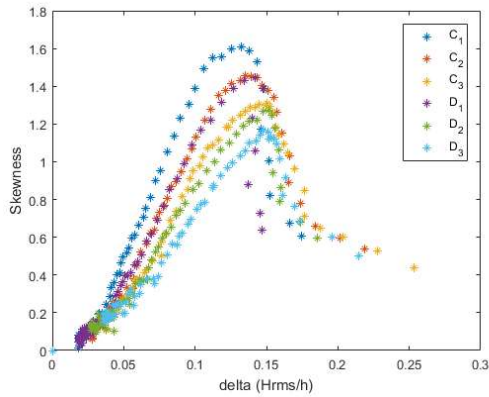


Figure 10: Skewness vs  $\delta$  – Random Wave Trials

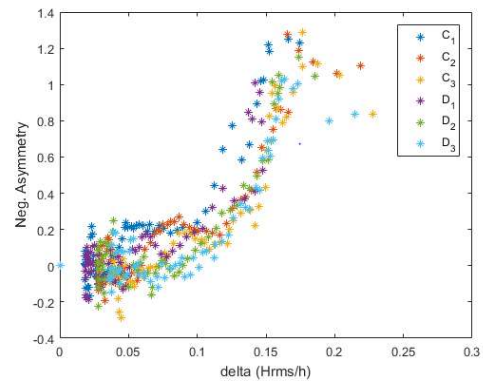


Figure 11: Asymmetry vs  $\delta$  – Random Wave Trials

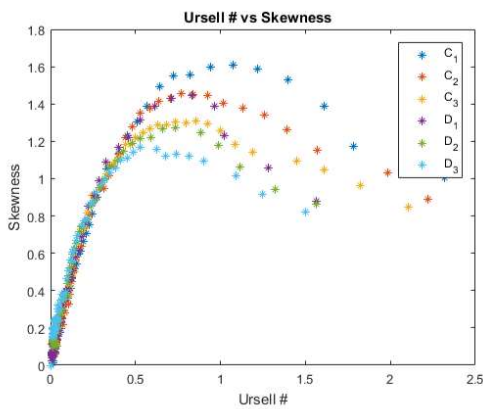


Figure 12: Ursell # vs Skewness – Random Wave Trials

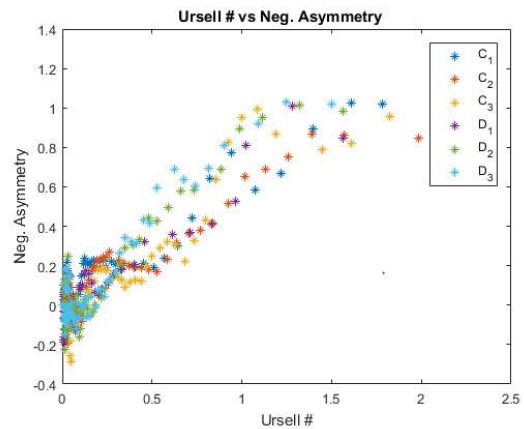


Figure 13: Ursell # vs Asymmetry - Random Wave Trials

For the random wave cases the plots have more well-defined trends, likely due to the wider area over which the wave breaking occurs. The skewness shown in figure 10 and 12 shows a steady increase as the waves approach shallower water until a maximum is reached, at which point a process occurs that decreases the skewness. In figures 11 and 13, the negative asymmetry is compared to  $\delta$  and the Ursell number in which the trend is

the same as the wave groups; as the depth decreases, the asymmetry becomes more negative.

Energy spectra at different depths were calculated and compared to each other as well. These plots are truncated at half the Nyquist frequency as that is the point we will use later in determining the log slope of these graphs. The data was divided into twelve realizations for the wave groups and 40 realizations for the random waves with 1024 points per realization; eight adjacent bands are averaged to smooth the data as shown below.

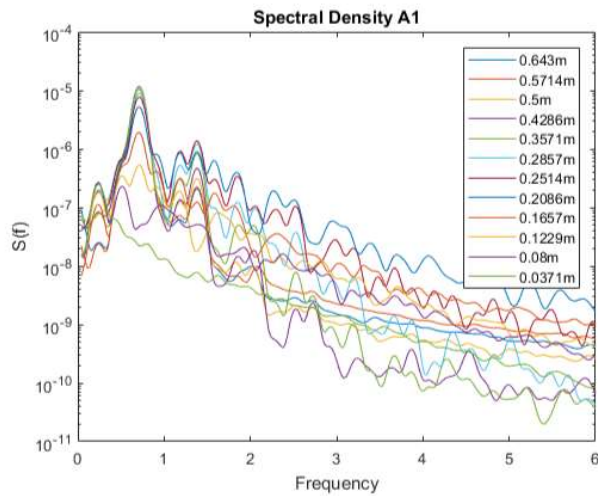


Figure 14: Spectral Density for A1 Group Wave



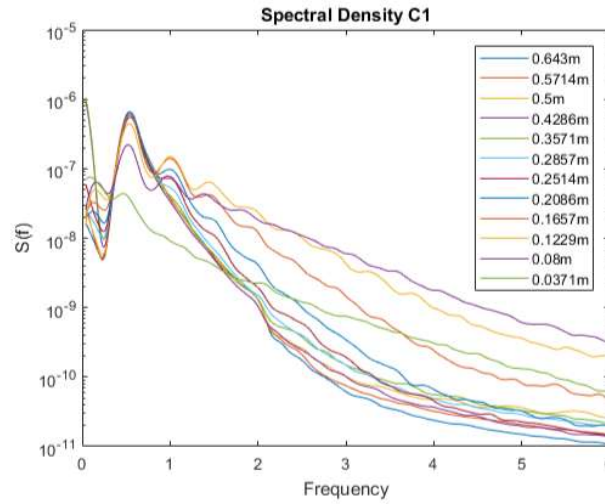


Figure 15: Spectral Density for C1 Random Wave

One observation is the fact that the wave groups have two main frequencies of high energy so the consequent harmonics have more energy in the shallower water. In the random wave case only the third harmonic appears to have a significant amount of energy and only in the shallower gauges. An equilibrium spectrum for each case and gauge was also calculated to see if the results matched Smith and Vincent (2003). The linear dispersion relation from chapter 1 was used to related wave frequency to wave number, then plotted versus the energy content. The results show that the mechanically driven waves perform similarly to the wind generated assumptions by Zakharov with a  $-4/3$  power law in the region ( $2.5k_p \leq k \leq 1/h$ ) but do not have a well-defined region characterized by Toba ( $k > 1/h$ ).

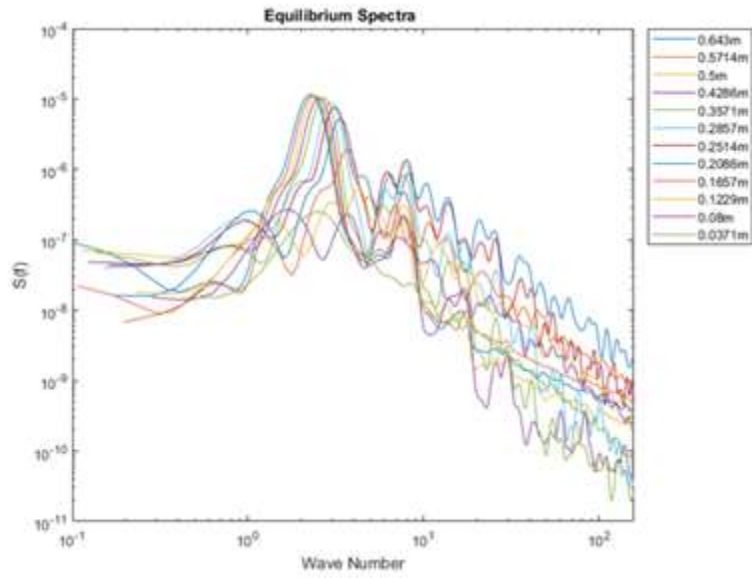


Figure 16: Equilibrium Spectra for A1 Group Waves

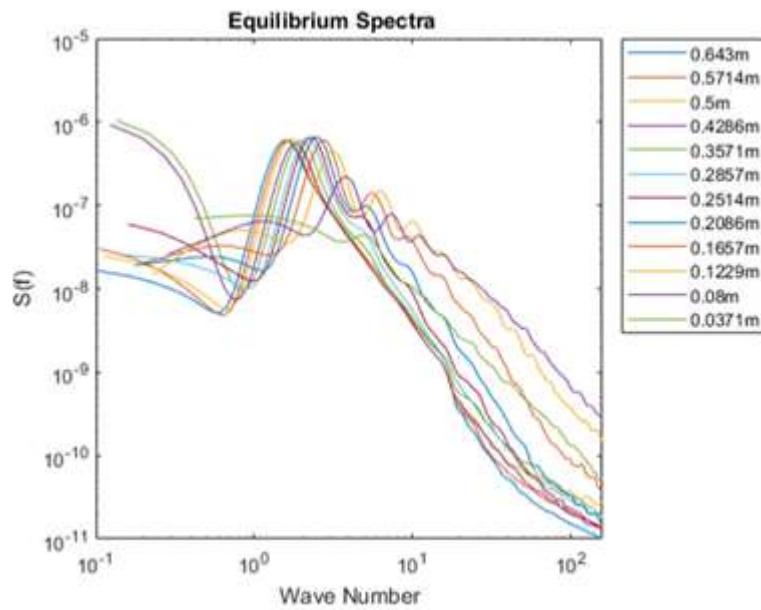


Figure 17: Equilibrium Spectra for C1 Random Wave

Values for  $\epsilon$  were calculated using equation 30, and the patterns of dissipation studied. An example time series is shown for  $\epsilon$  below for one of the areas in which breaking dissipation is occurring.

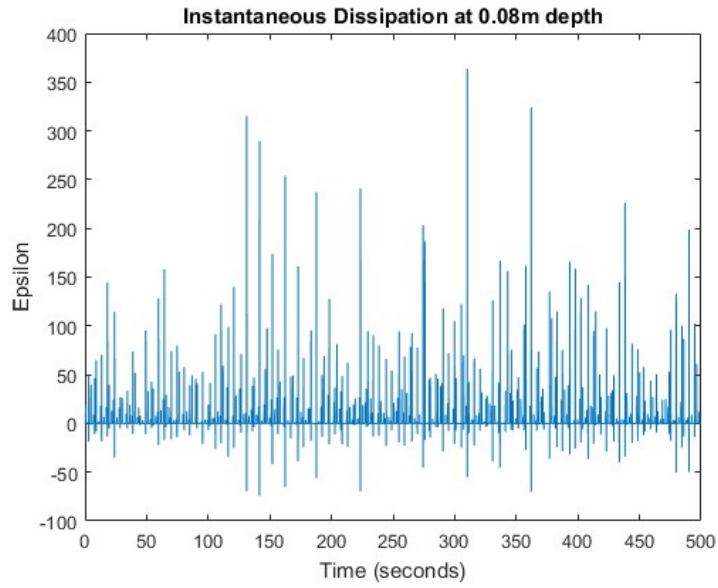


Figure 18: Instantaneous Dissipation for A1 Group Wave

The graph shows that using the formulation of Kaihatu et al. (2007) the dissipation occurs as ‘spikes’ in the time series, the spectrum of which appears to be “white” (equal energy across many frequencies).

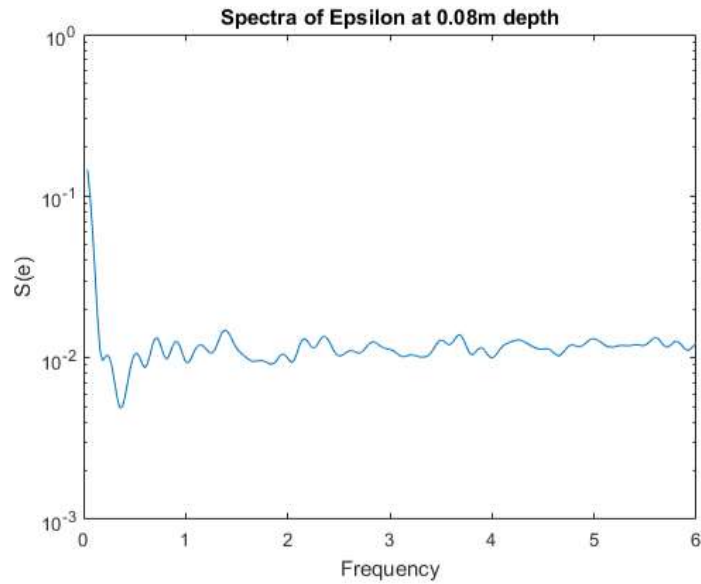


Figure 19: Spectral Analysis of  $\epsilon$  A1

The values for  $\epsilon$  have been processed in two ways; first a spectral analysis is done as shown on figure 19, and second the values for  $\epsilon$  can be placed into a probability density function for the relative probability of each integer value of instantaneous dissipation. For the spectral analysis of  $\epsilon$ , the same number of band averages and points per realization was used as in the energy spectra (8 and 1024 respectively). The probability of a single value for  $\epsilon$  dwarfed the remaining instantaneous dissipation values, resulting in the probability density function shown on the next page.

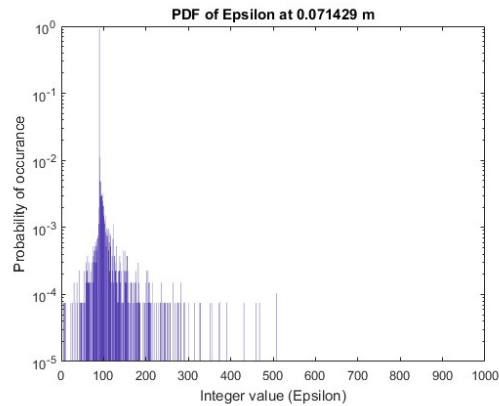


Figure 20: PDF of  $\epsilon$  Group Wave A1

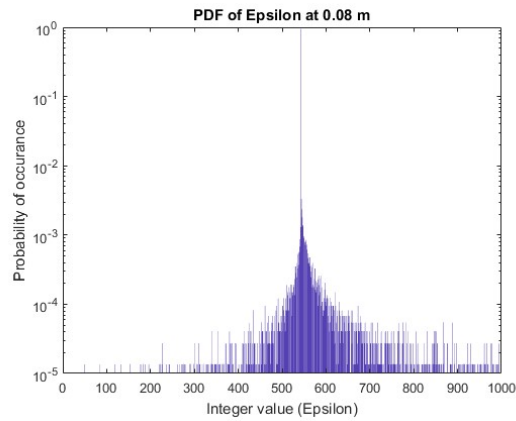


Figure 21: PDF of  $\epsilon$  Random Wave C1

The data for these probability functions required a log-y axis plot to allow the percentages of values other than the highest visible. The probability of a single value being dominant remains relatively constant throughout the breaking and swash zones of both group waves and random waves (Although the exact value that  $\epsilon$  is changes). Shown below is a graph containing the values of the highest probability  $\epsilon$  at each depth, and below that the corresponding percent chance at each depth that any instantaneous dissipation will be that value.

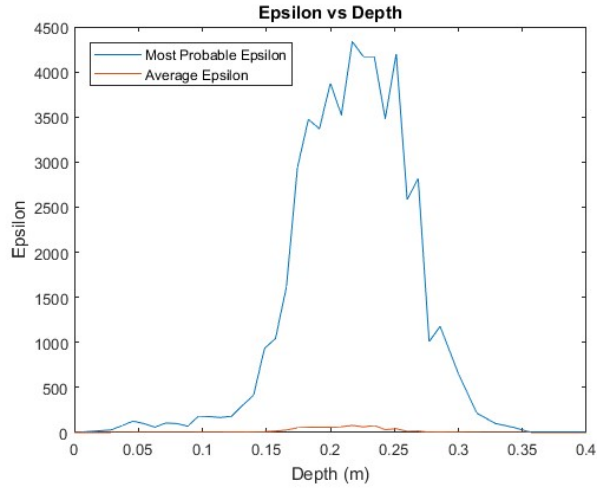


Figure 22: Most Probable  $\epsilon$  Values for Group Wave B2

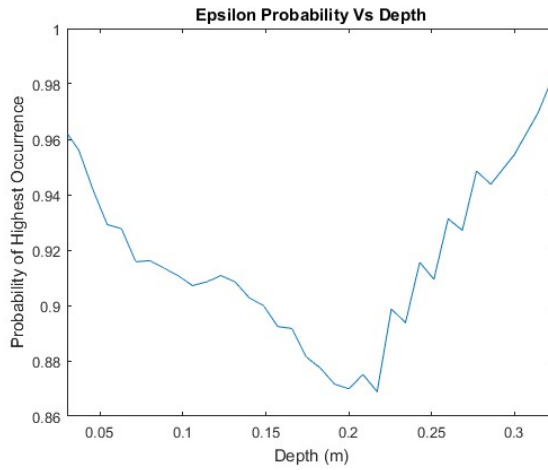


Figure 23: Probability of Most Probable  $\epsilon$  for B2

Dissipation rates, denoted  $\alpha$ , were calculated using equation 31 the energy and  $\epsilon$  spectra for each wave trial. The slopes of  $\alpha$  for each trial was calculated using a power fit. This lead to some interesting patterns for comparing the group and random wave cases.

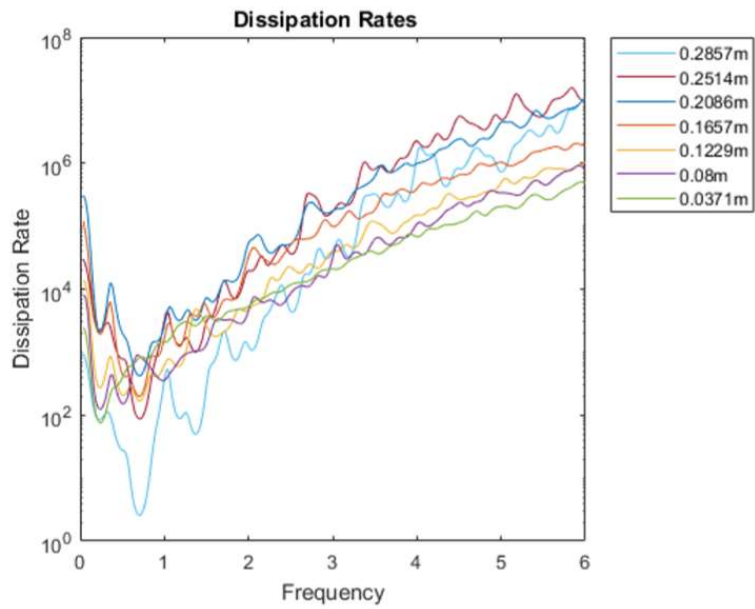


Figure 24: Dissipation Rates A1

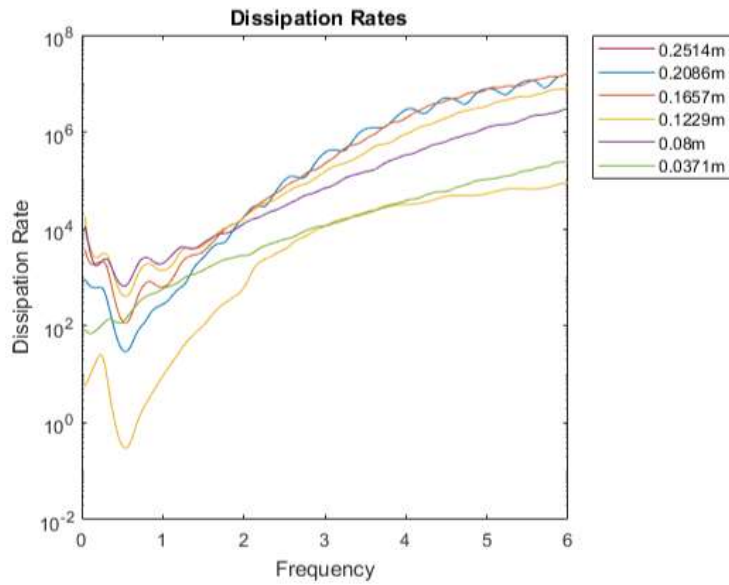


Figure 25: Dissipation Rates C1

The lowest value of dissipation shown in figures 24 and 25 occur at a low frequency, which translates to a longer wave using the dispersion relation. These long

waves do not lose energy as rapidly as the higher frequency short waves inside the coastal zone. Remarkably the trend of the wave groups and random waves is seemingly identical in these plots. The dissipation rates and spectral energy plots were then processed with a log-log plot and a linear interpolation to ascertain the dependency of  $\alpha$  and  $S(f)$  with frequency and water depth.

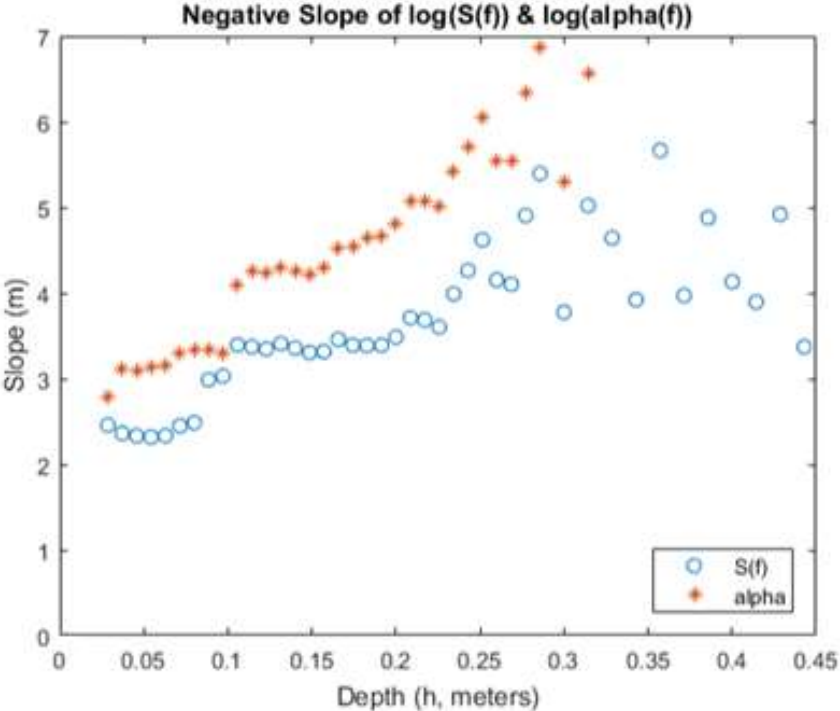


Figure 26: Dissipation Log Slopes A1



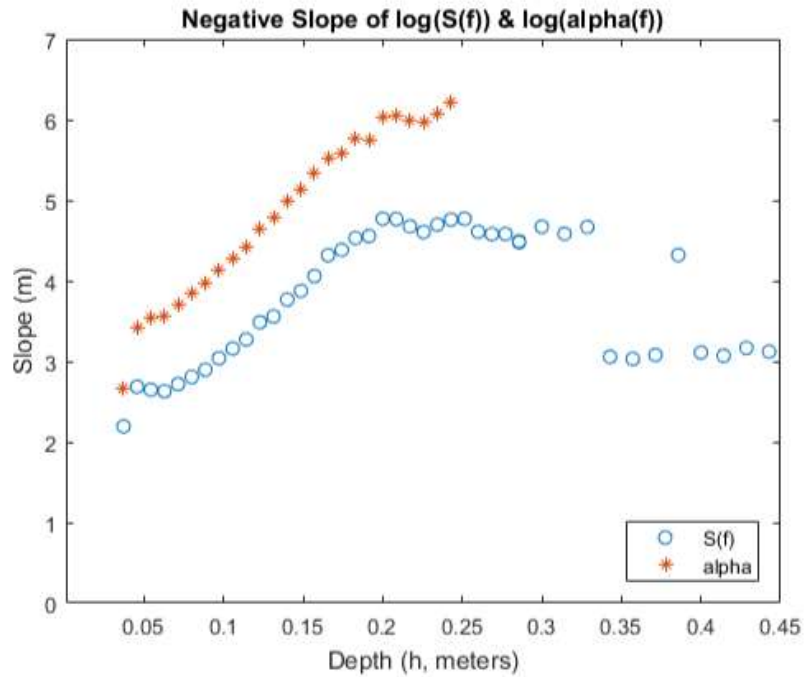


Figure 27: Dissipation Log Slopes C1

The dependency on frequency to  $\alpha$  and  $S(f)$  is shown on these graphs as a power law (the power of the frequency dependence). The wave groups on figure 26 comprise of two regions mainly, from deep water to 0.1m depth and in the zone shallower than 0.1m. The random waves have a much more structured slope that seems to have a linear relation.

There were a total of fifteen experiments recorded (nine group wave trials and six random wave trials) the average dissipation slope for each depth was computed with error bars to show the deviation of each point. The points were then linearly interpolated again to relate  $\alpha$ ,  $S(f)$ , and  $h$ .

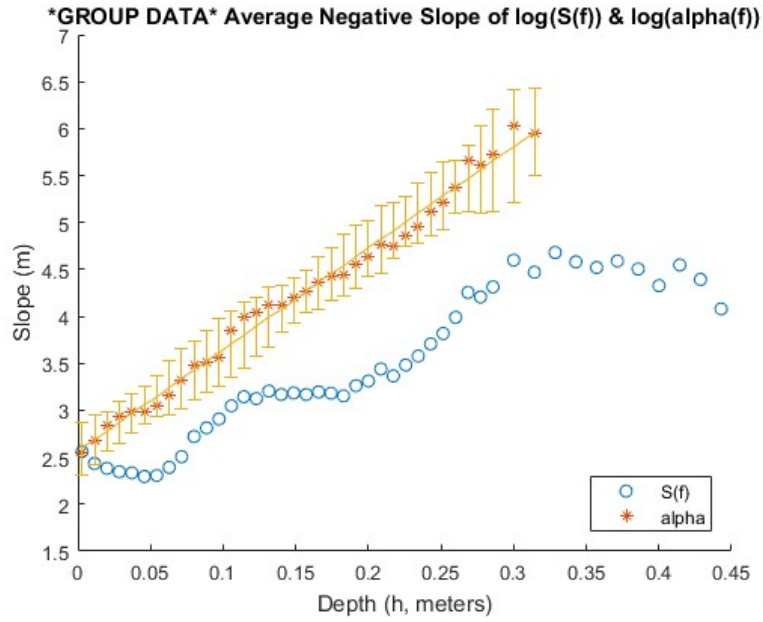


Figure 28: Averaged Log Dissipation Slopes for 9 Group Wave Trials

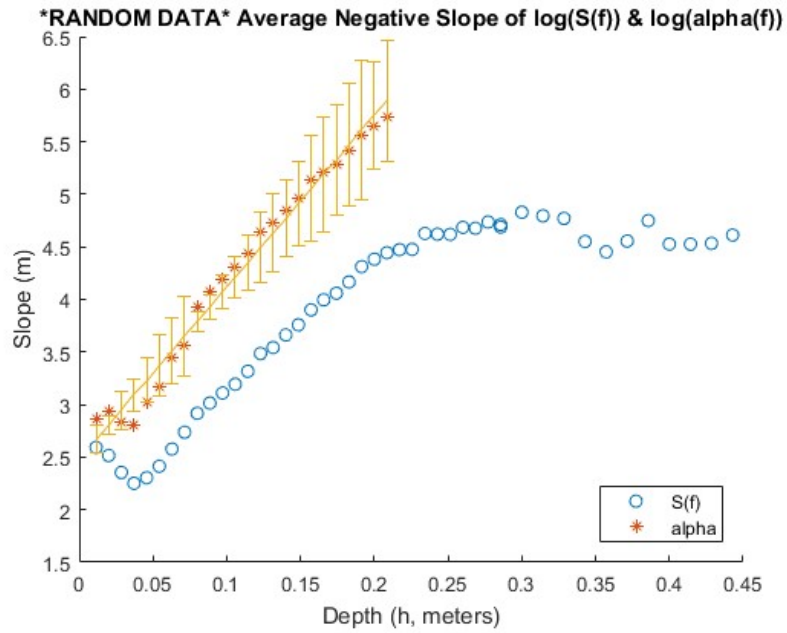


Figure 29: Averaged Dissipation Slopes for 6 Random Wave Trials

A remarkable difference between the random waves and wave groups is that the random waves have a high deviation at deeper water but then go towards an asymptote whereas the group waves have a high deviation at deeper water and then again at shallower water.

### **3.3 Discussion**

Skewness and asymmetry calculated for each wave trial can be used to determine when waves break. Values of maximum skewness indicate that the waves have a very steep slope on the front face, which occurs before and during breaking as the crest topples over into the trough. Values of asymmetry have been shown to be inversely proportional to the water depth, likely due to shallow water waves causing set-up so that more water is above the mean water level.

Ursell numbers and  $\delta$  were compared to the skewness and asymmetry. They have three regions in which there are different processes dominant inside the coastal zone. First there seems to be a 1 to 1 relation between the values, indicating that breaking has not occurred, and the pure shoaling described in chapter one is happening. Then the graphs start to even out, describing the start of dissipation due to the steepness of the wave face. Afterwards energy is lost and the loss in wave height is displayed as a loss in the dimensionless parameters  $\delta$  and Ursell number. All four plots for both random and wave groups show a direct proportionality between these dimensionless parameters. This is to be expected since  $\delta$  is a measure of relative wave height and is divided by the water depth and the Ursell number is a function of  $\delta$ .

The spectral analysis of each wave gauge and trial are useful in categorizing each type of wave. The wave groups are comprised of two distinct frequency peaks, whereas the random trials have only 1 peak as indicative of the physical phenomenon researched prior. Then the spectral plots are useful in comparing the dissipation slopes to a characteristic of each type of wave. The negative log slope can inform the dependency of the spectral energy with the frequency. Equilibrium spectra are useful to compare to work done by Zakharov and Toba for the different ranges of frequency dependence. The  $4/3$  power law proposed by Zakharov for wind driven spectra appears to also apply to the mechanically driven ones created during this experiment.

Values of  $\epsilon$  were calculated match the previous studies done using the Zelt model. The spiked nature of  $\epsilon$  shows that dissipation using this model is injected at discrete times. This method causes the related Fourier analysis to output a sort of ‘white noise’ or that there is no dependency of  $\epsilon$  on the frequency. The probability of each integer value of  $\epsilon$  was calculated and plotted on figure 20 and 21. These show a difference from previous statistics that involved dissipation arranging values in more of a Gaussian distribution with a single value very high occurrence value. This trend in  $\epsilon$  may invalidate the use of the Zelt model in the study of wave dissipation since it varies dramatically from the Rayleigh distribution predictions from lumped dissipation models.

Values of  $\alpha$  have a correlation to frequency dependent on the water depth apparent in the power fit figures 26 and 27. The values of  $\alpha$  increase rapidly at lower frequencies then evens out causing equal dissipation per frequency at the higher ranges. This is similar for both the wave groups and random waves. This is due to long waves

dissipating energy at a slower rate than shorter, higher frequency waves. These long waves then carry more energy into the nearshore region and have significant impact on the beach front. For the wave groups in figure 24 there is a significant drop from the long wave frequencies into the frequencies mechanically generated by the wave maker.

The slopes of  $\alpha$  and energy spectra were compared to each other and asymptotic behavior was found. In previous research conducted by Chen et al. (1997) and Kaihatu et al. (2007) the asymptotic behavior of this power should be equal to two. Both figures 28 and 29 trend  $\alpha$  and  $S(f)$  towards 2.5 which may be an error in the data analysis discussed in the conclusion. The random waves trend towards higher dependency on frequency as the water depth increases, compared to the wave groups. This is likely due to the two frequencies of waves interacting and breaking at different water depths. Using the averaged slope figures 28 and 29 and the asymptotic behavior described by previous studies, it is shown that  $\alpha$  is proportional to frequency and water depth as follows.

Equation 40: Random Wave Dissipation Dependency

$$\alpha_n \propto f^{(2+16.35h)}$$

Equation 41: Group Wave Dissipation Dependency

$$\alpha_n \propto f^{(2+10.82h)}$$

where  $f$  is the frequency in Hz and  $h$  is the water depth in meters. Furthermore, curve fitting using dimensionless parameters to calculate  $A$  in equation 42 was completed to form a general approach for approximating higher frequency dissipation characteristics. The error between the new formulation and the calculated dependency was 8.8% for group waves and 1.5% for random waves.

Equation 42: Combined Dissipation Dependency

$$\alpha_n \propto f^{(2+A*h)}$$

Equation 43

$$A = \frac{\pi}{4} * \frac{Ursell\# * \delta}{Hrms}$$

Equation 43 is comprised of average values over all the wave trials for the *Ursell #*, *Hrms*, and  $\delta$  which means that water depths inside of  $\delta$  and *Ursell #* will use an average water depth over the surf zone unlike equation 42 which uses a specific water depth in the surf zone for calculations. Using this parameter, *A*, the dissipation slopes at each depth can be estimated with respect to the frequency. The figures 30 and 31 below show the relationship between the actual dissipation dependency at each depth to the formulation in equation 43, for group and random waves respectively and using the same *y* intercept for each.

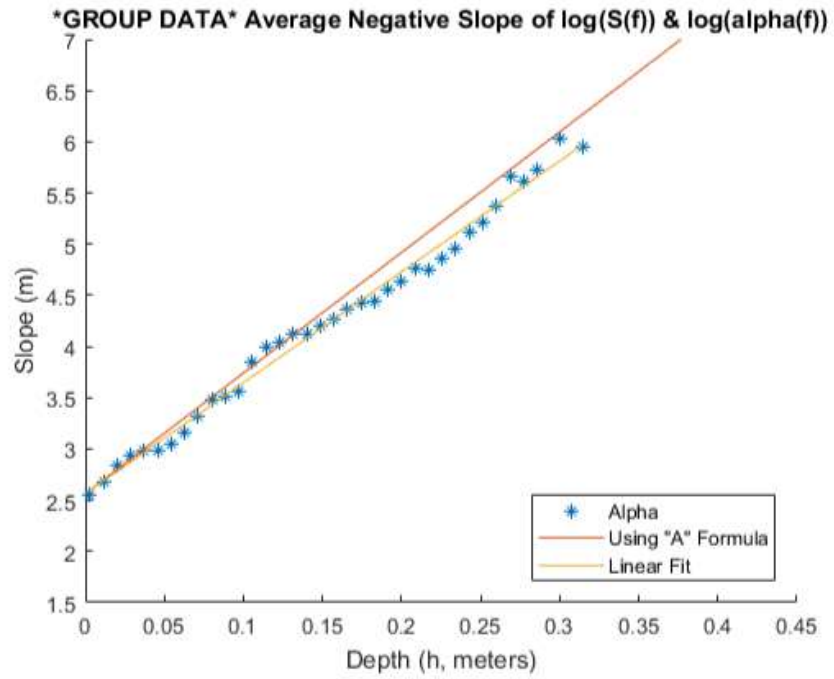


Figure 30: Comparison of Equation 43 to results; group wave trials

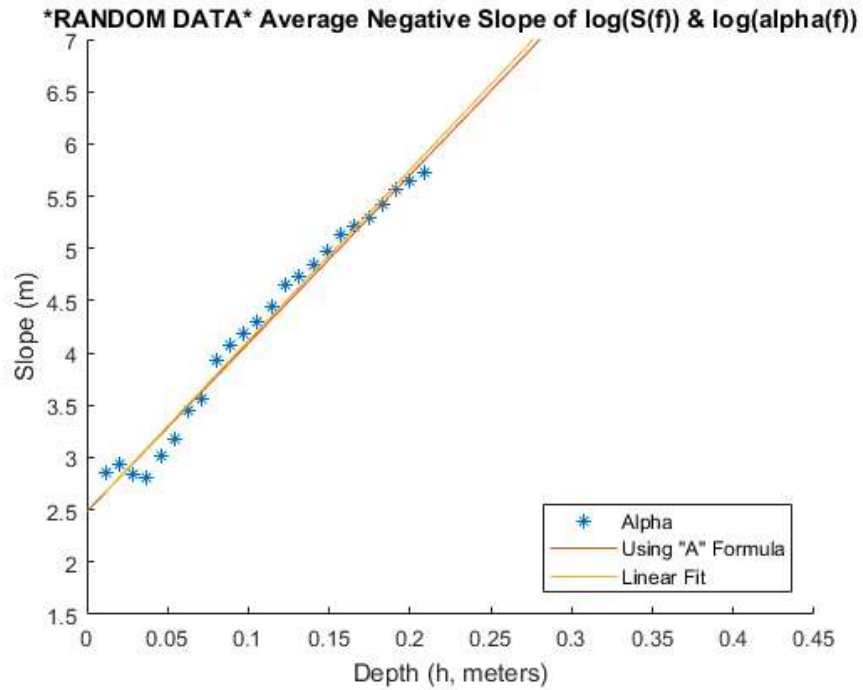


Figure 31: Comparison of Equation 43 to results; random wave trials

## CHAPTER IV

### CONCLUSION

The dissipation characteristics of the wave groups and random waves were shown to have a similar asymptotic behavior as the water depth tended towards zero, but a much different dependency in deeper water depths. The probability of each  $\epsilon$  value using the Zelt model has a single value of very high occurrence that may invalidate the processes described in chapter 2 for the study of wave dissipation. This probability density function of  $\epsilon$  varies substantially from the lumped dissipation results from Rayleigh distributions. The assumptions of the Zelt model that the dissipation is based on a turbulent bore could be incorrect in dealing with shallow water wave breaking or the linear relationship described so that waves can be processed via time derivatives instead of spatial derivatives might need to include higher order terms.

The averaged graphs tending towards an asymptote of 2.5 instead of 2 could be an error in the data processing where points are chosen for linear interpolation, the spectral width, or the small values of  $kh$  (relative wave number) in the wave tank. The points were chosen using the lowest dissipation frequency to half the Nyquist frequency, or for the energy spectra, the highest energy frequency to half the Nyquist frequency. This difference could also be due to the limited fetch distance for coupling of waves in the wave basin.

The formulation in equations 39 and 40 are for mechanically driven waves due to a piston, further research should be done for wind driven waves to see if the trends



match. The fetch distance on waves created under a wave maker also could skew the frequency dependency, in other words the waves might not have sufficient space in the tank to fully develop before shoaling and subsequently breaking.

## REFERENCES

- Bailard, James A. (1981) An Energetics Total Load Sediment Transport Model for a Plane Sloping Beach. *Journal of Geophysical Research*, 86, C11
- Battjes, J. A., and J. P. F. M. Janssen (1978), Energy Loss and Set-Up due to Breaking of Random Waves, *Proceedings of the 16<sup>th</sup> International Conference of Coastal Engineering*, p. 569, American Society of Civil Engineers, New York
- Bowen, G. D., and J. T. Kirby (1994) Shoaling and Breaking Random Waves on a 1:35 Laboratory Beach, *Tech. Rep. CACR-94-14*, Center for Applied Coastal Resources, American Society of Civil Engineers., Hamburg, Germany.
- Collins, J. I., Probabilities of Breaking Wave Characteristics, *Proceedings of the 13<sup>th</sup> International Conference Coastal Engineering*, pp. 399-412, American Society of Civil Engineers, New York
- Goda, Y. (1975) Irregular Wave Deformation in the Surf Zone, *Coastal Engineering Journal*, 18, 13-26
- Kaihatu J. M., and J. T. Kirby (1995), Nonlinear Transformation of Waves in Finite Water Depth, *Phys. Fluids*, 7(8), 1903-1914
- Kaihatu, J., and Safty, H. M. (2011). Spectral Description Of Energy Dissipation In Breaking Wave Groups. *Coastal Engineering Proceedings*, 1(32), 19.  
doi:10.9753/icce.v32.waves.19
- Kaihatu, J. M., Veeramony, J., Edwards, K. L., & Kirby, J. T. (2007). Asymptotic Behavior of Frequency and Wave Number Spectra of Nearshore Shoaling and

- Breaking Waves. *Journal of Geophysical*, 112, C06016  
doi:10.1029/2007JC003817
- Kuo, C. T., and S. T. Kuo (1974), Effect of Wave Breaking on Statistical Distribution of Wave Heights, *Proc. Civil Engineering. Oceans*, 3, 1211-1231
- Longuet-Higgins, Michael S. (1952). On the Statistical Distribution of the Heights of Sea Waves. *Journal of Marine Research*, 9, 245-266
- McCowan, J., "On the Highest Wave of Permanent Type", *Philos. Mag. J. Sci.*, Vol 38
- Noorloos, V. (2003) *Energy Transfer between Short Wave Groups and Bound Long Waves on a Plane Slope*. (MS Thesis) Delft University of Technology, Delft, Netherlands.
- Smith, J. M. and Vincent, C. L. (2003) Equilibrium Ranges in Surf Zone Wave Spectra, *Journal of Geophysical Research*, 108, No. C11, 3366
- Thornton, E. B., and Guza, R. T. (1983). Transformation of Wave Height Distribution, *Journal of Geophysical Research*, 88, 5925-5938
- Toba, Y. (1973), Local Balance in the Air-Sea Boundary Processes on the Spectrum of Wind Waves, *Journal Oceanography Society Japan.*, 29, 209-220.
- Weggel, J. R. (1972), "Maximum Breaker Height" *J. Waterways, Harbors Coastal Engineering Division., ASCE*, Vol. 98, No. WW4
- Zakharov, V. (1999), Statistical Theory of Gravity and Capillary Waves on the Surface of a Finite-Depth Fluid, *Eur. J. Mech. B Fluids*, 18, 327-344.
- Zelt, J. A. (1991), The Run-up of Nonbreaking and Breaking Solitary Waves, *Coastal Engineering.*, 15, 205-246

APPENDIX A  
GRAPHS FOR A1 CASE

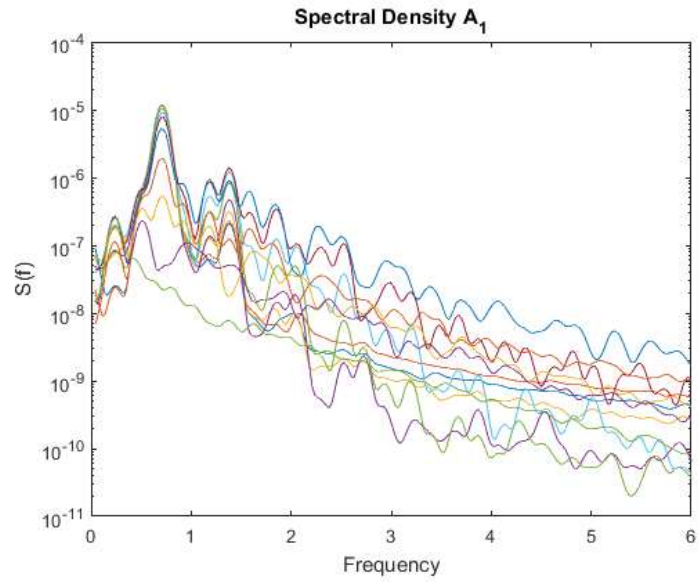


Figure 32: Spectral Density A1

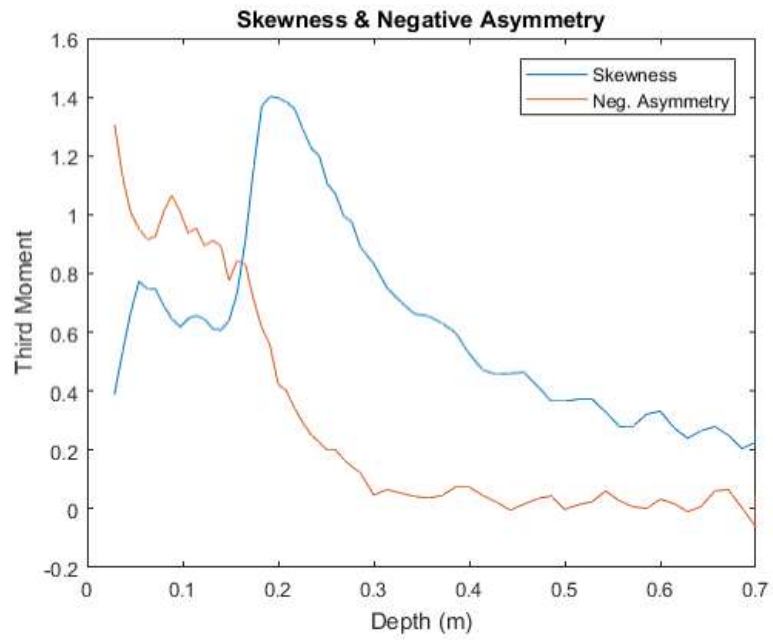


Figure 33: Skewness & Neg. Asymmetry A1

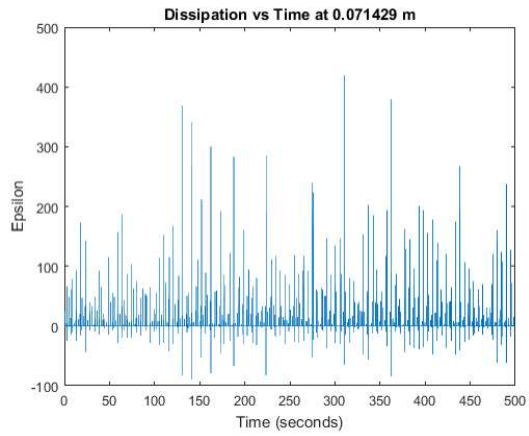


Figure 34: Values of  $\epsilon$  A1

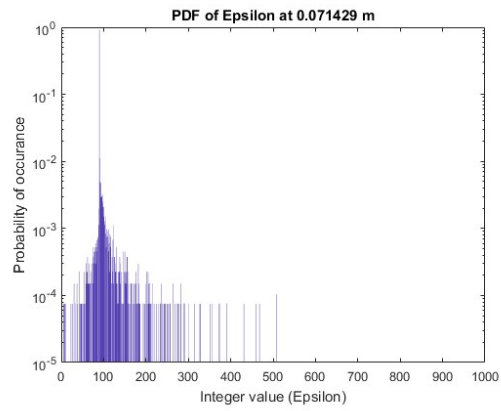


Figure 35: PDF of  $\epsilon$  A1

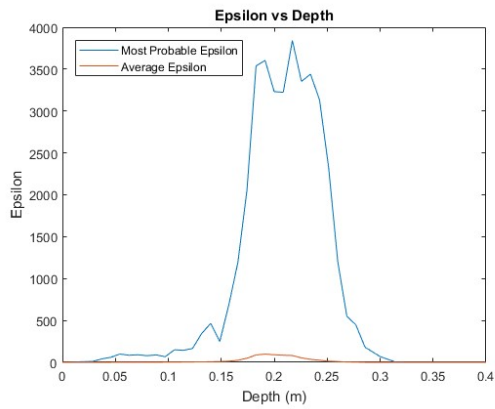


Figure 36: Highest Probability  $\epsilon$  vs Depth A1

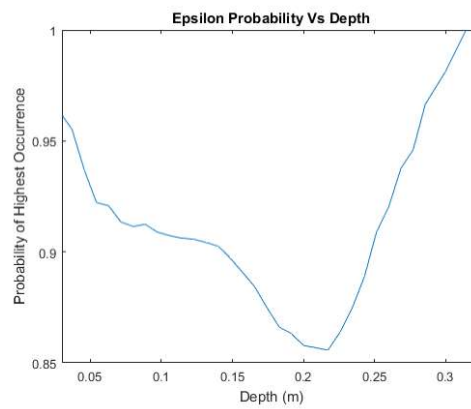


Figure 37: Most Probable  $\epsilon$  A1

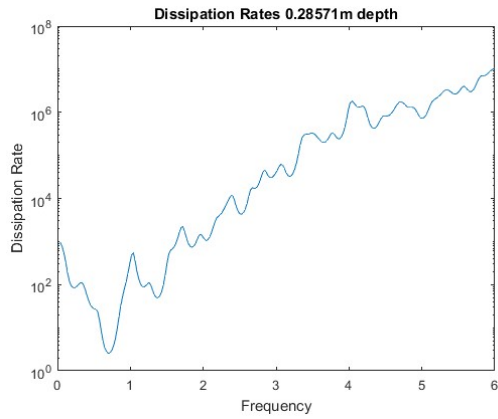


Figure 38: Dissipation Rate at 0.285m A1

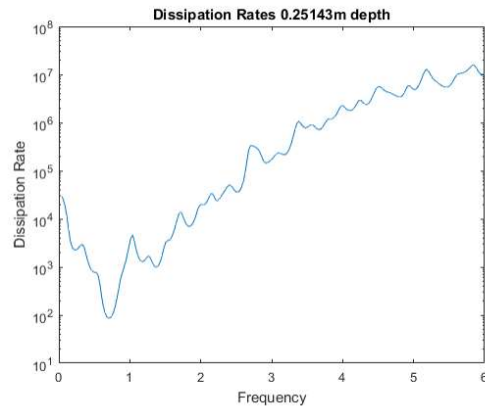


Figure 39: Dissipation Rate at 0.251m A1

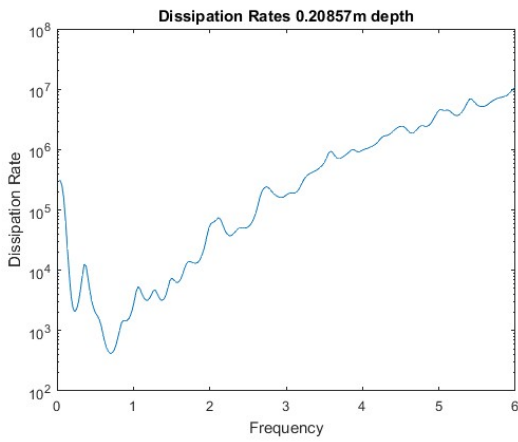


Figure 40: Dissipation Rate at 0.209m A1

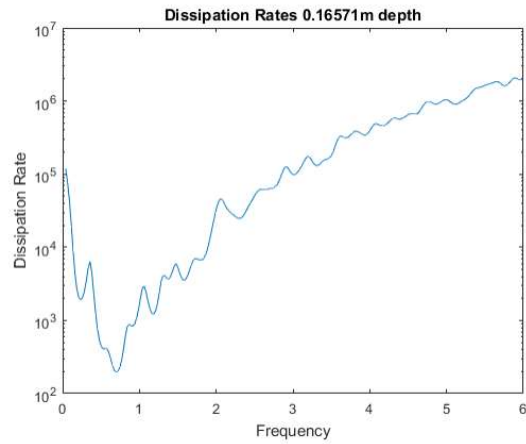


Figure 41: Dissipation Rate at 0.166m A1

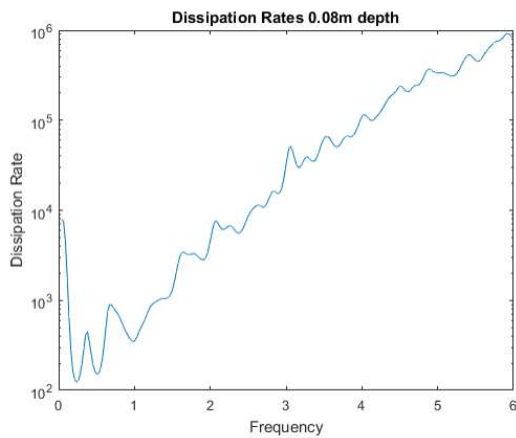


Figure 42: Dissipation Rate at 0.08m A1

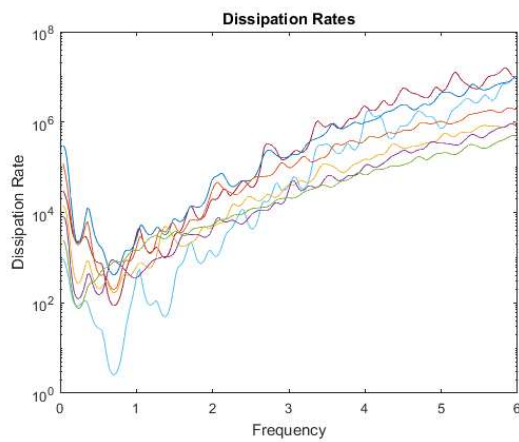


Figure 43: Dissipation Rates A1

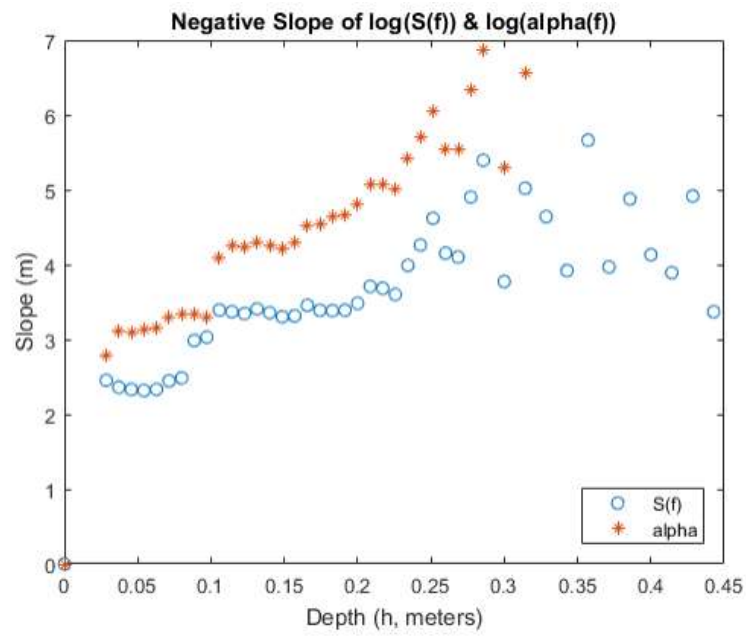


Figure 44: Log-Log Slope of Dissipation Rates A1

APPENDIX B  
GRAPHS FOR B2 CASE

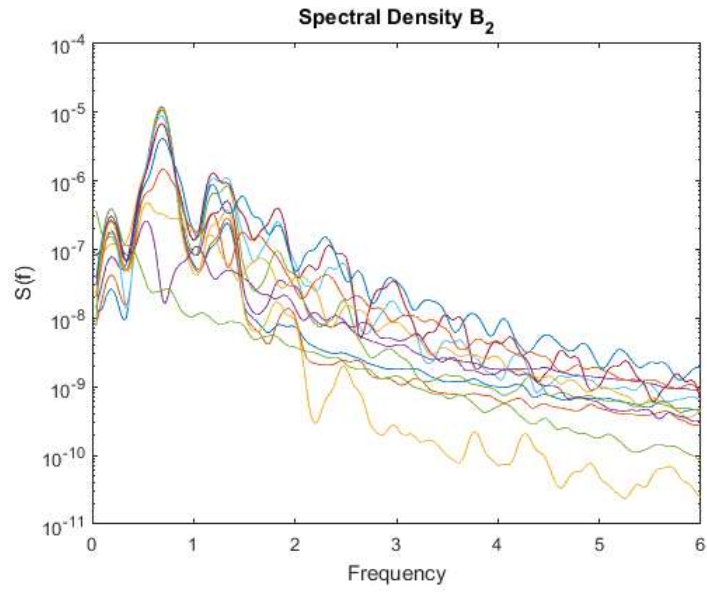


Figure 45: Spectral Density B2

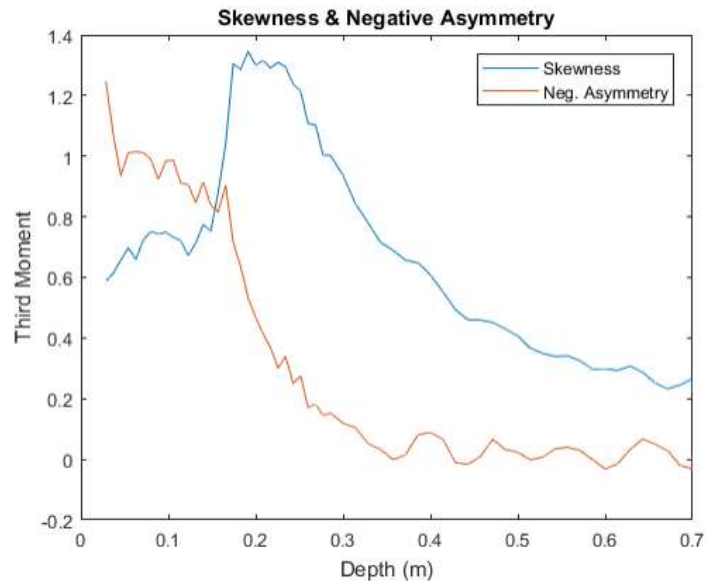


Figure 46: Skewness and Asymmetry B2



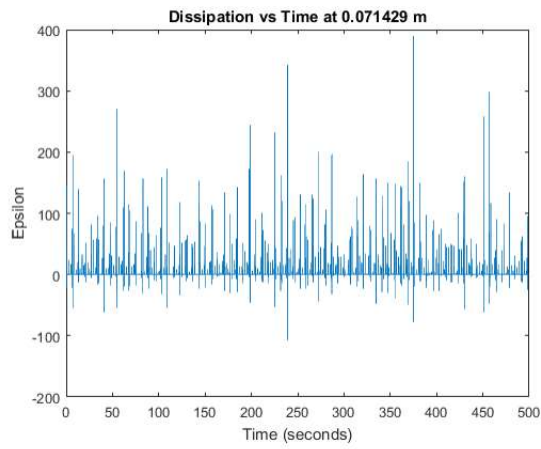


Figure 47: Values of  $\epsilon$  B2

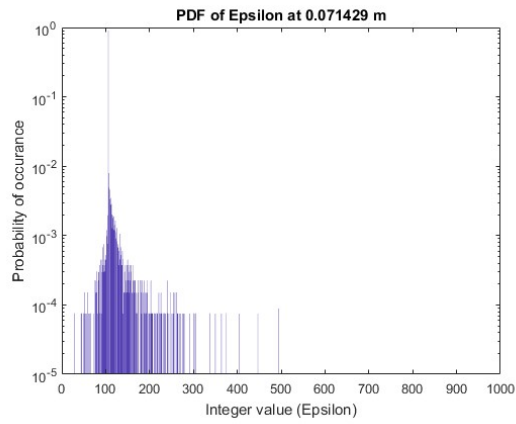


Figure 48: Probability Density Function of  $\epsilon$  B2

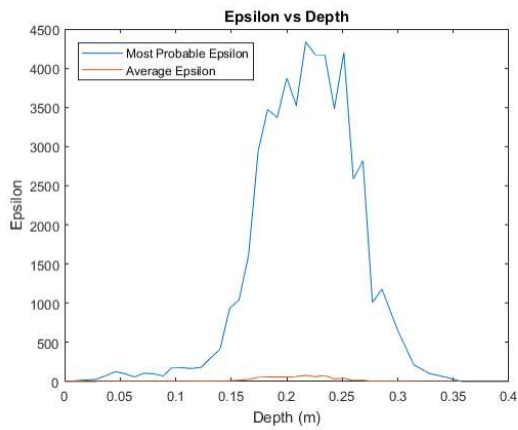


Figure 49: Most Probable  $\epsilon$  vs Depth B2

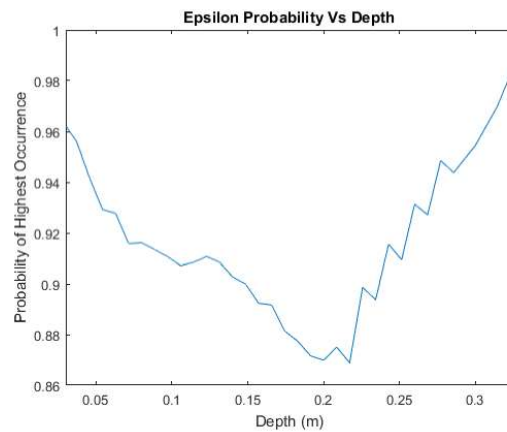


Figure 50: Most Probable  $\epsilon$  Probability B2

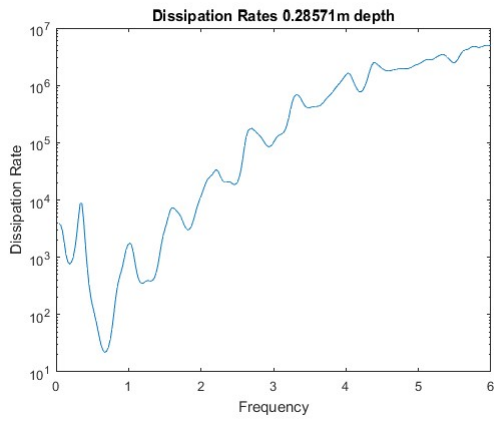


Figure 51: Dissipation Rate at 0.286m B2

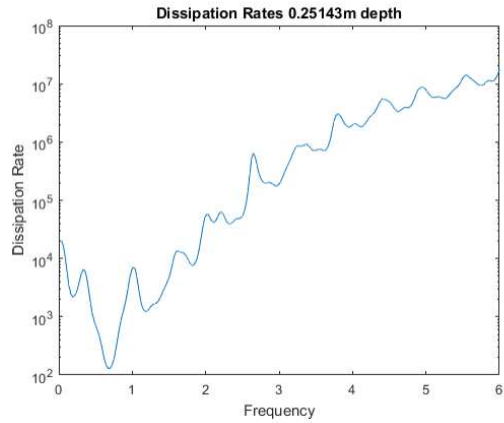


Figure 52: Dissipation Rate at 0.251m B2

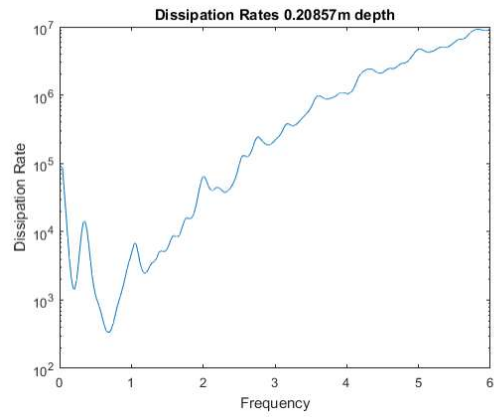


Figure 53: Dissipation Rate at 0.209m B2

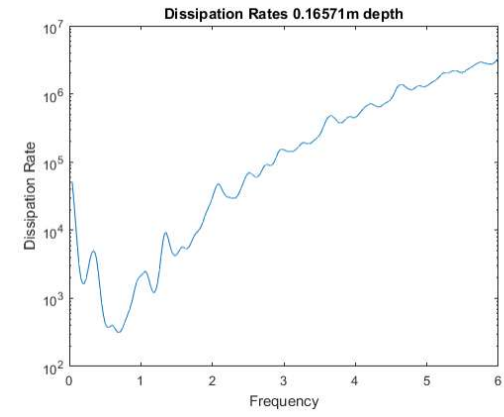


Figure 54: Dissipation Rate at 0.166m B2

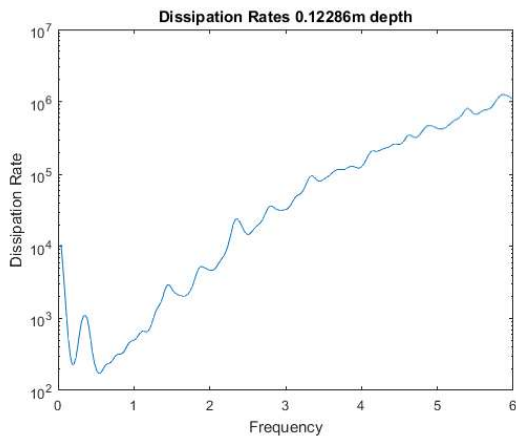


Figure 55: Dissipation Rate at 0.123m B2

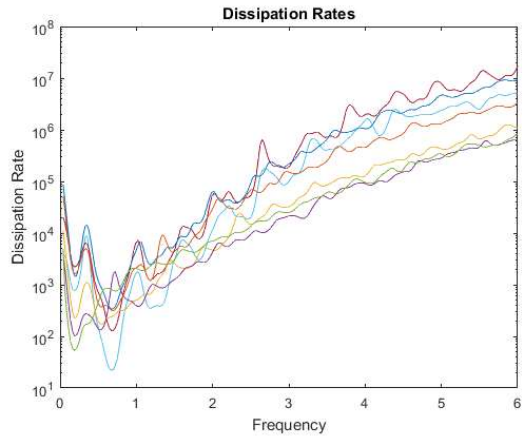


Figure 56: Dissipation Rates B2

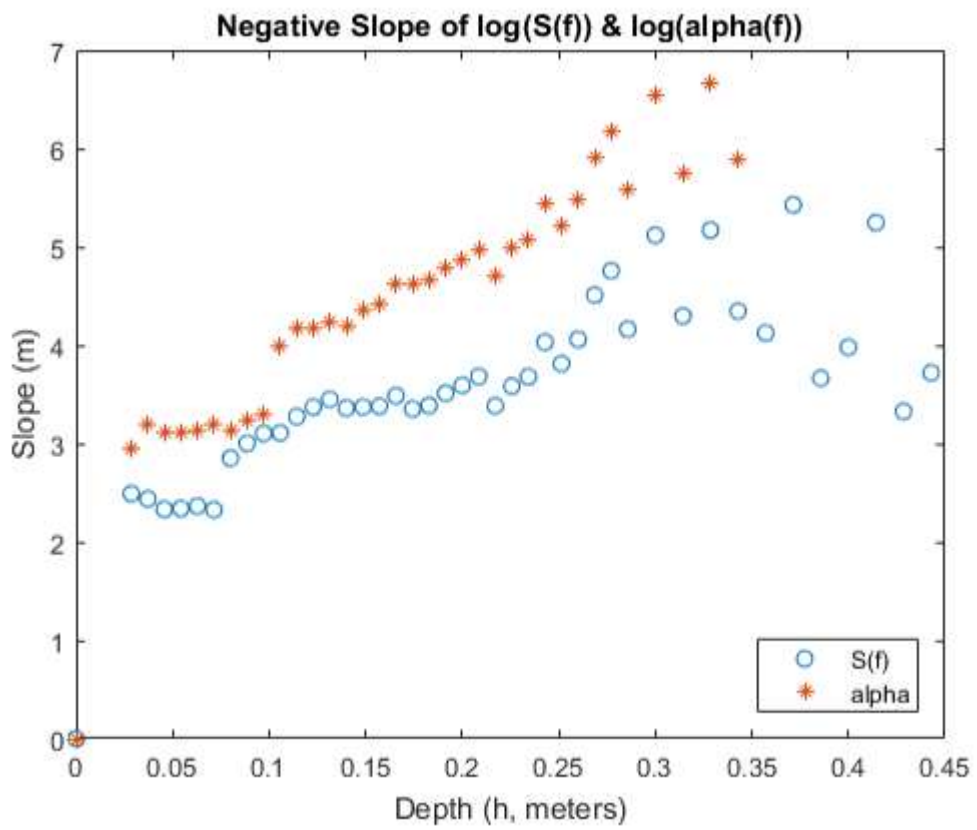


Figure 57: Log-Log Slope of Dissipation Rates B2

APPENDIX C  
GRAPHS FOR C1 CASE

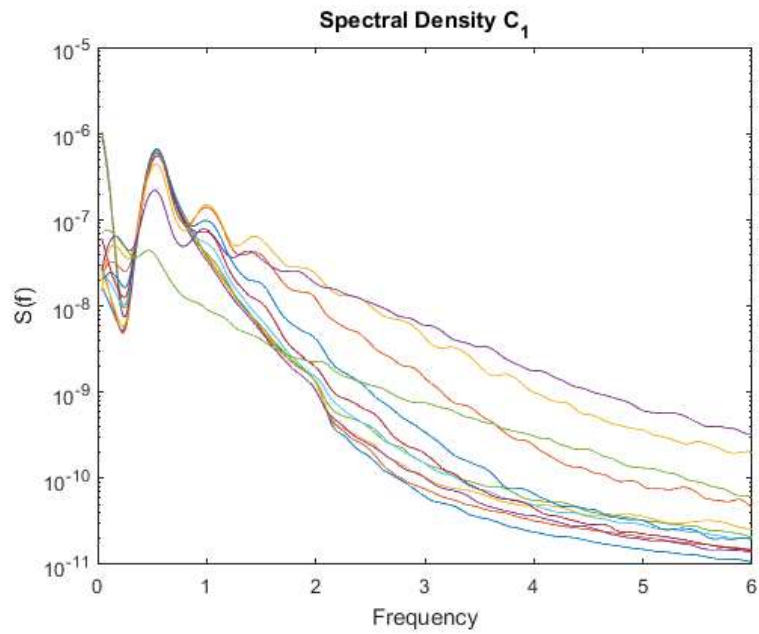


Figure 58: Spectral Density C1

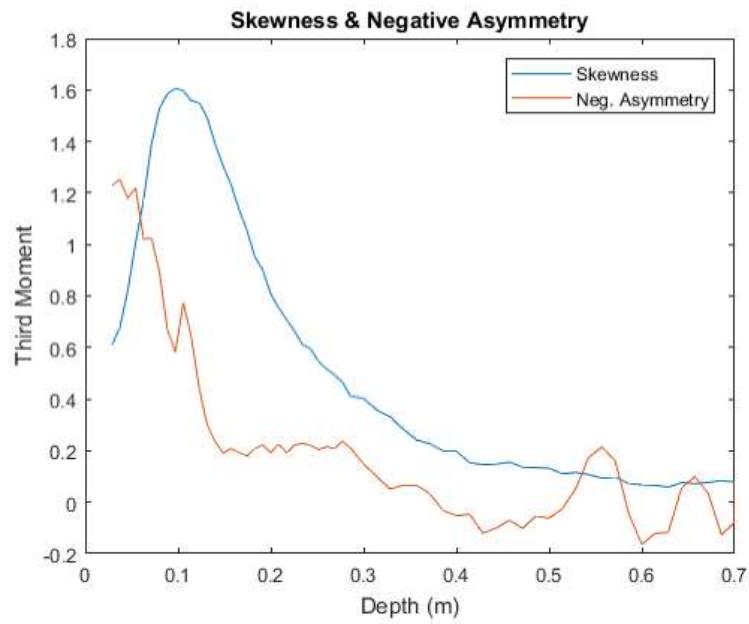


Figure 59: Skewness and Asymmetry C1

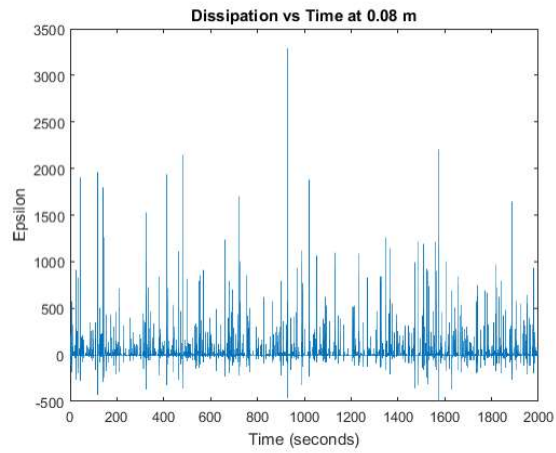


Figure 60: Values of  $\epsilon$  C1

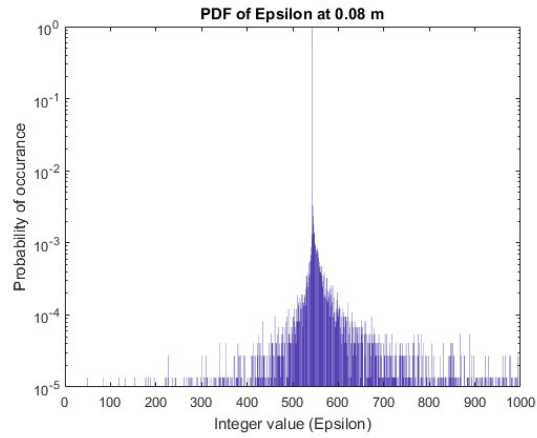


Figure 61: Probability of  $\epsilon$  C1

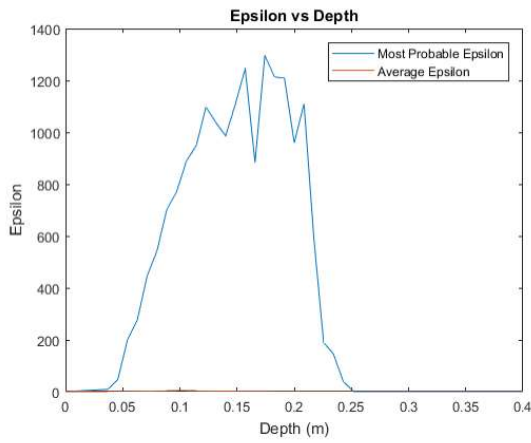


Figure 62: Most Probable  $\epsilon$  vs Depth C1

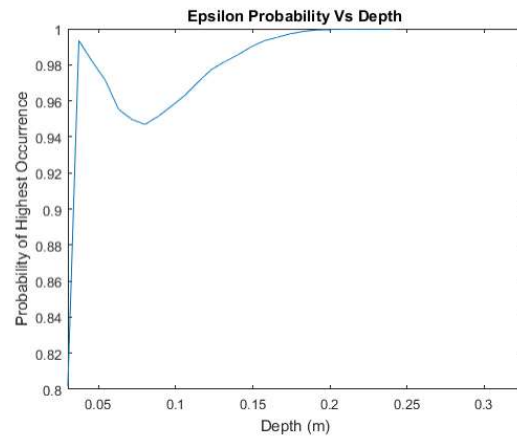


Figure 63: Probability of  $\epsilon$  C1

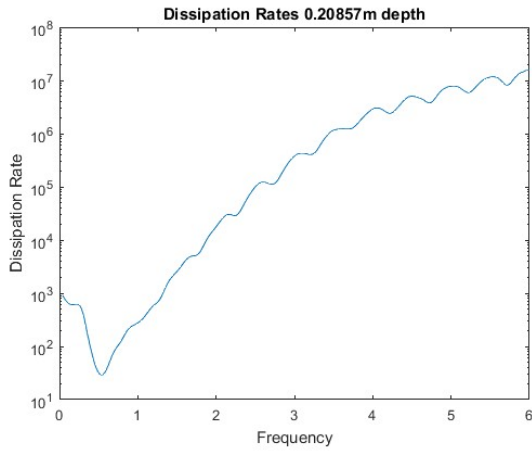


Figure 64: Dissipation Rate at 0.209m C1

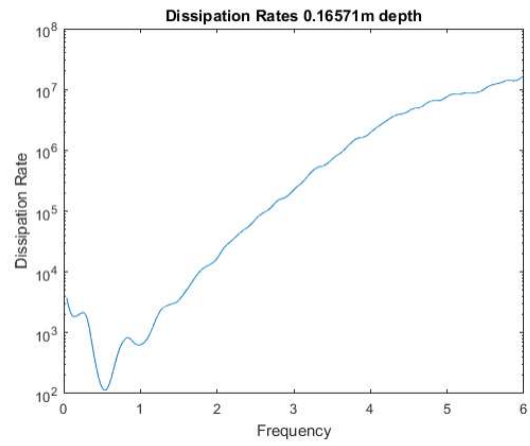


Figure 65: Dissipation Rate at 0.166m C1

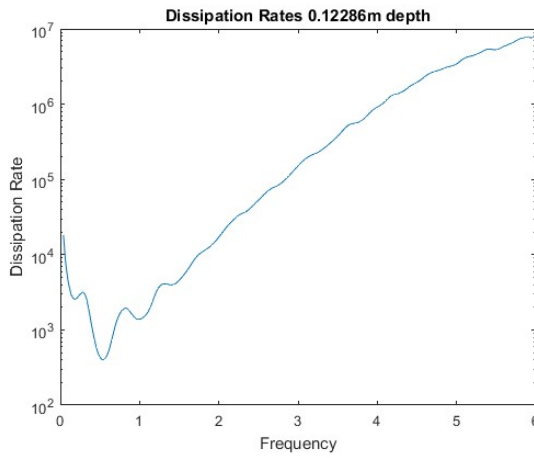


Figure 66: Dissipation Rate 0.123m C1

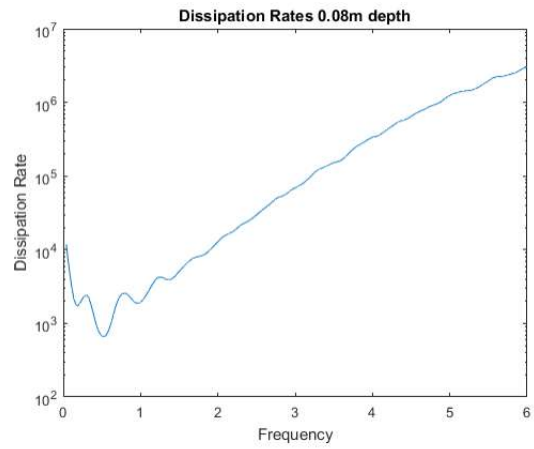


Figure 67: Dissipation Rate at 0.08m C1

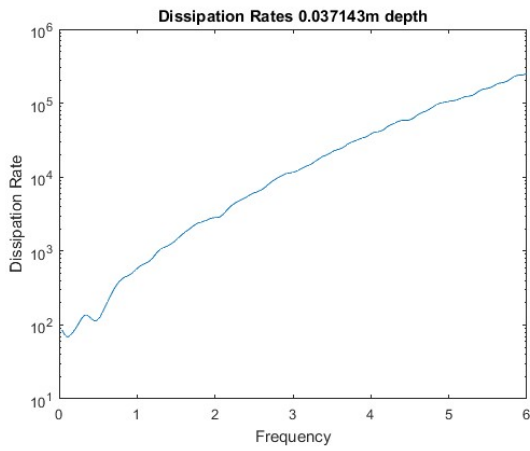


Figure 68: Dissipation Rate at 0.037m C1

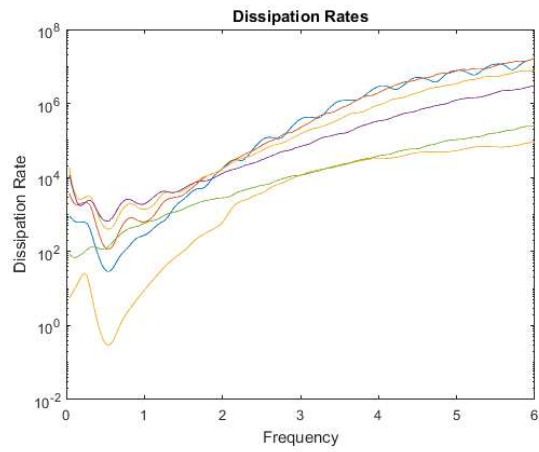


Figure 69: Dissipation Rates C1

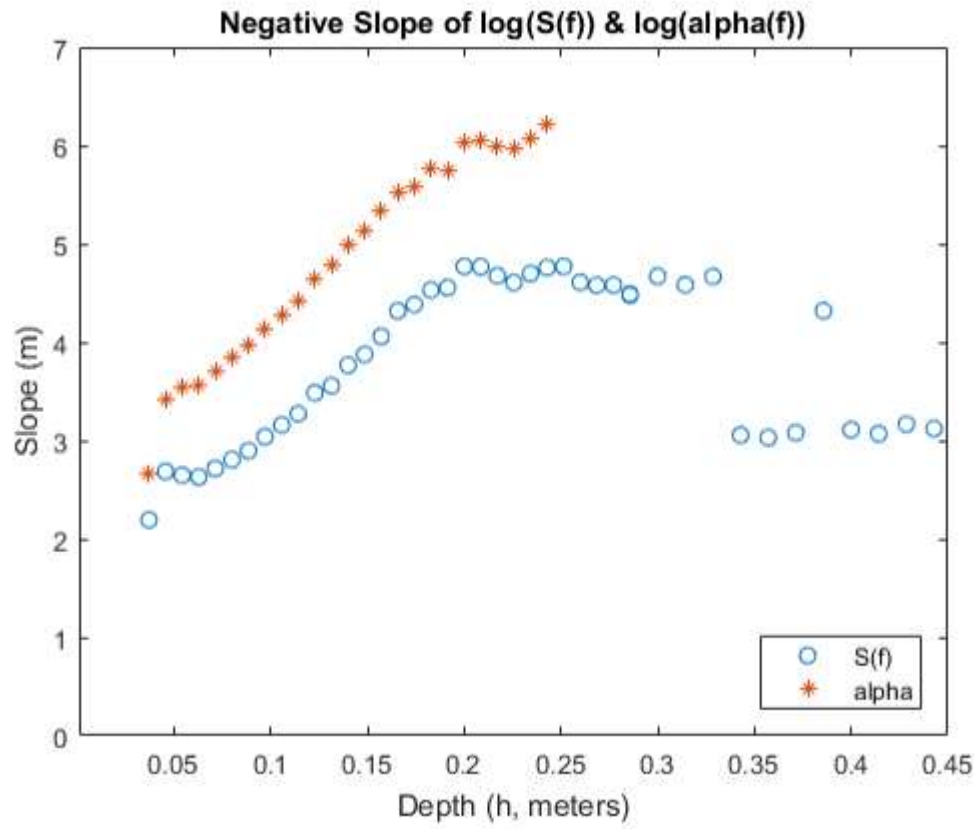


Figure 70: Log-Log Slopes of Dissipation Rate C1

APPENDIX D  
GRAPHS FOR D1 CASE

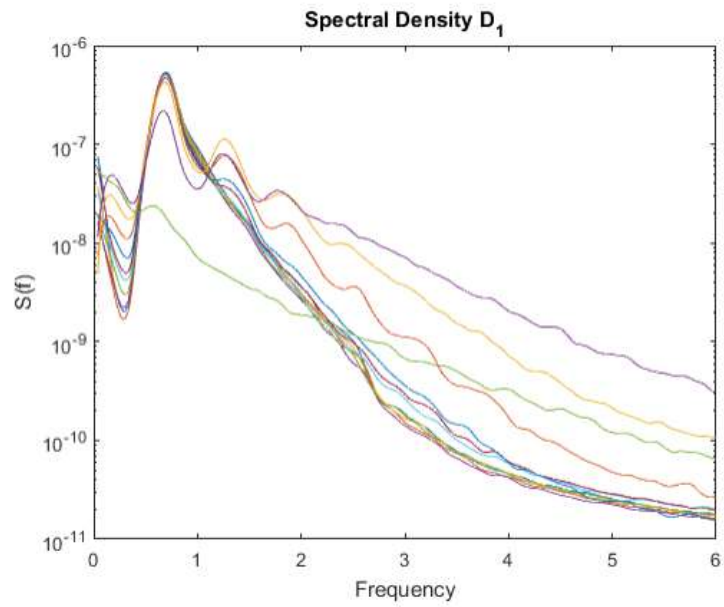


Figure 71: Spectral Density D1

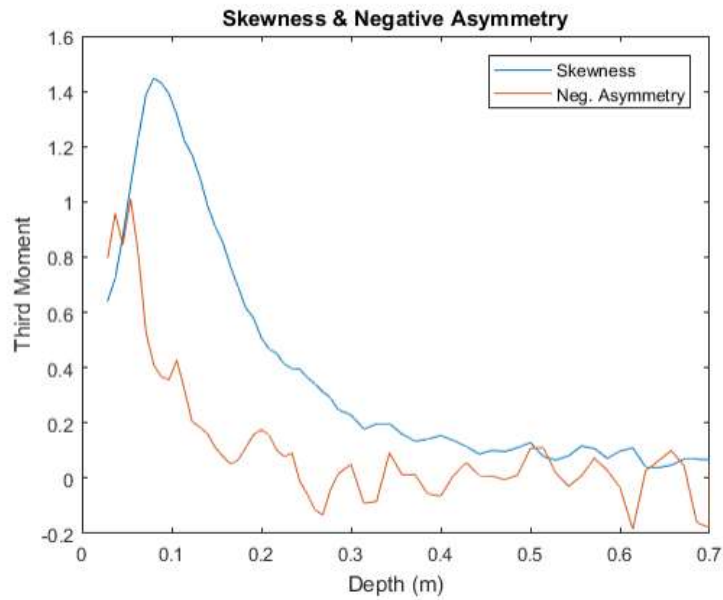


Figure 72: Skewness and Asymmetry D1



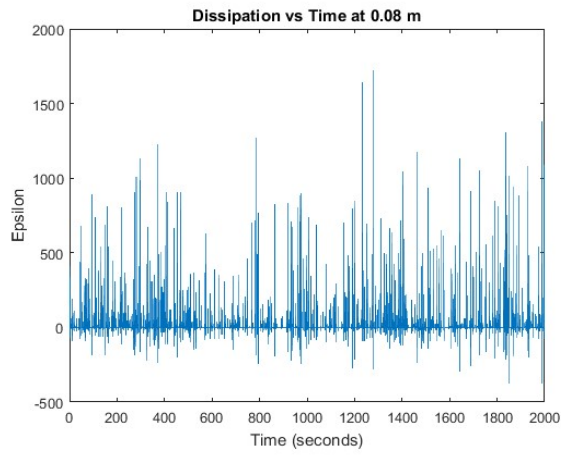


Figure 73: Values of  $\epsilon$  D1

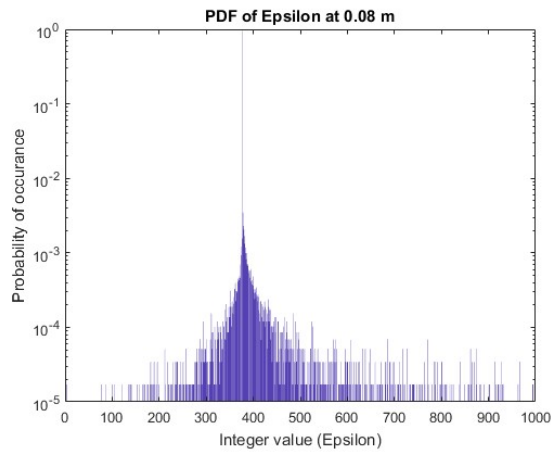


Figure 74: Probability Density Function of  $\epsilon$  D1

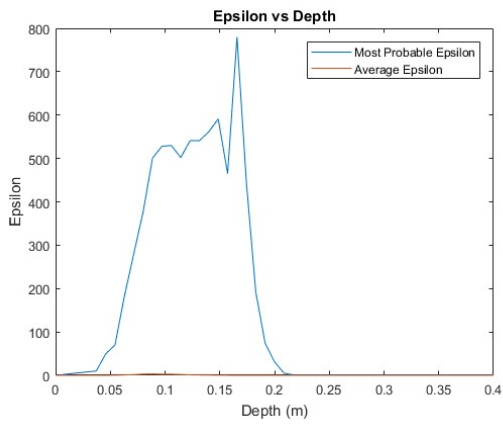


Figure 75: Most Probable  $\epsilon$  vs Depth D1

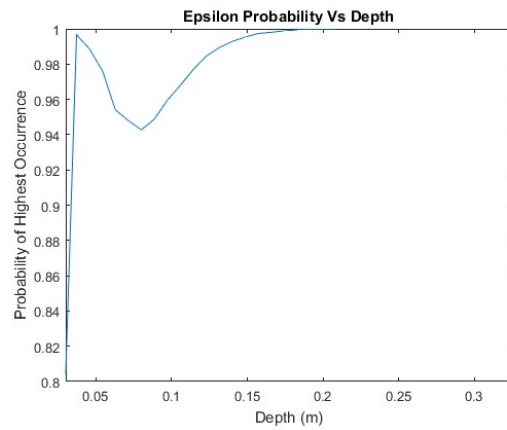


Figure 76: Probability of  $\epsilon$  vs Depth D1

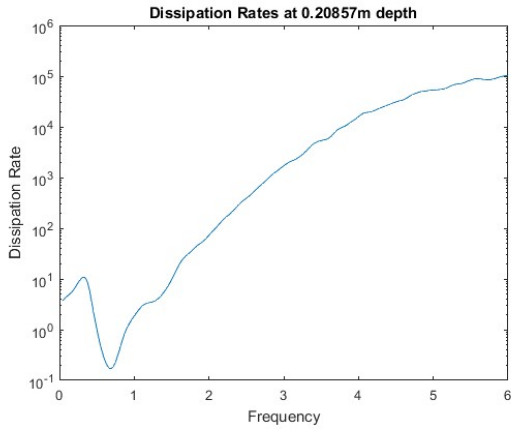


Figure 77: Dissipation Rate at 0.209m D1

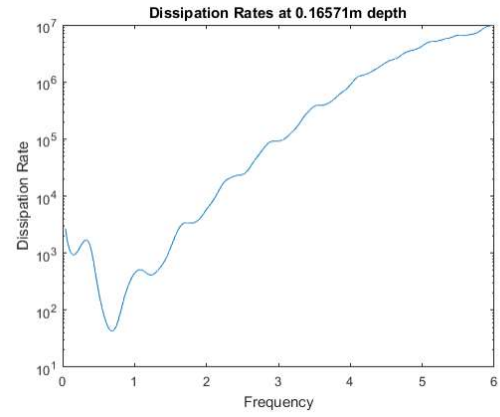


Figure 78: Dissipation Rate at 0.166m D1

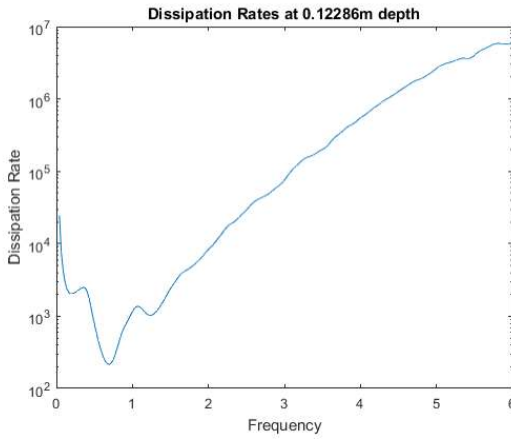


Figure 79: Dissipation Rate at 0.123m D1

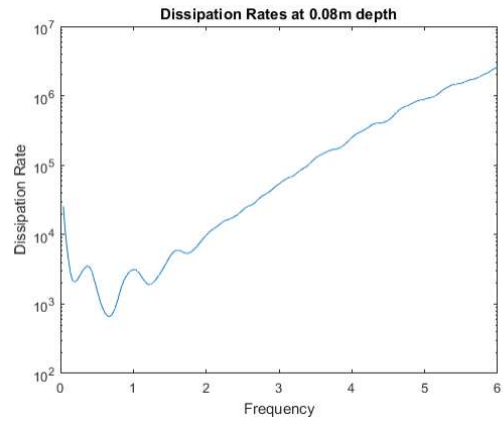


Figure 80: Dissipation Rate at 0.08m D1

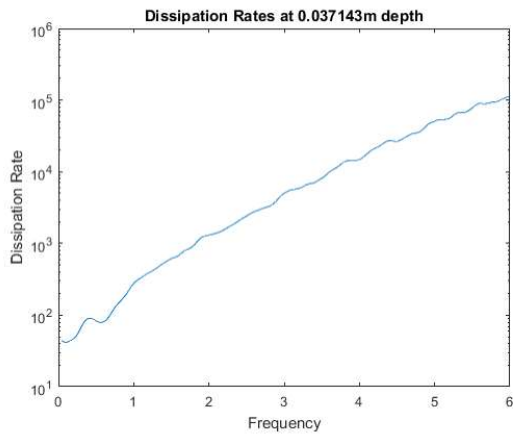


Figure 81: Dissipation Rate at 0.037m D1

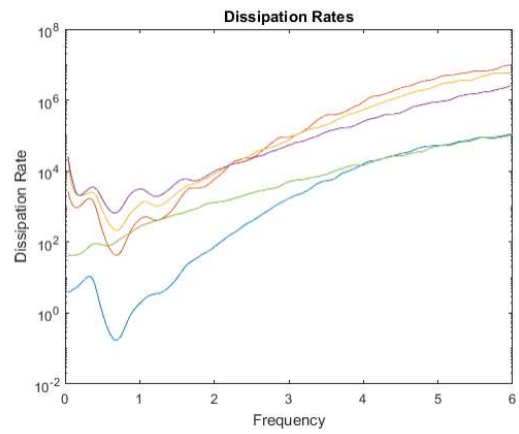


Figure 82: Dissipation Rates D1

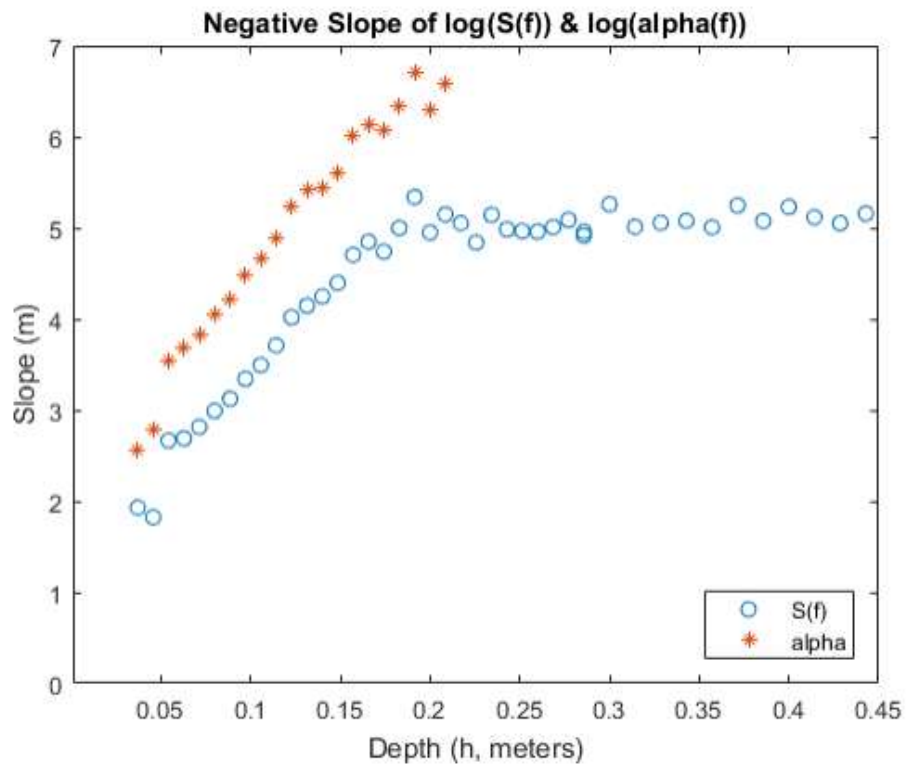


Figure 83: Log-Log Slopes of Dissipation Rates D1